Enabling Technologies for Broadband In-Band On-Channel Digital Radio

Zixia Hu

A dissertation
submitted in partial fulfillment of the
requirements for the degree of

Doctor of Philosophy

University of Washington

2012

Reading Committee:

Hui Liu, Chair

Sumit Roy

Payman Arabshahi

Program Authorized to Offer Degree:
Electrical Engineering

University of Washington

Abstract

Enabling Technologies for Broadband In-Band On-Channel Digital Radio

Zixia Hu

Chair of the Supervisory Committee:
Professor Hui Liu
Department of Chair

Due to inadequate spectrum resources and increasing demands for high quality multimedia services, traditional analog broadcasting is being migrated into digital radio around the world. This dissertation focuses on the development of several innovative broadcasting technologies and the design of so-called Broadband Digital Radio (BDR) system, which is suitable for digital audio and data broadcasting in FM and AM channels. The new broadcasting system synergistically integrates frequency hopping, LDPC coding, hierarchical modulation and band aggregation techniques to increase the data rate, improve spectrum efficiency, and at the same time, provide the spectrum flexibility necessary in high quality audio and multimedia services.

One of the key features in the BDR is the powerful hierarchical modulation scheme that offers significant performance enhancement over existing schemes (e.g., DVB-T). In this dissertation, we present a novel decoding algorithm for the hierarchical modulation. Unlike the traditional hierarchical demodulation approaches which suffer from serious inter-layer interference (ILI), the proposed method exploits the structure information of the secondary layer to mitigate the ILI impairment, thereby offers significant gains in reception performance.

For the digital network, frequency planning is needed as in other digital broadcasting signals. Most importantly, the single frequency network (SFN) architecture will be used in the BDR deployment. The hierarchical modulation technique is also adopted in the SFN

to provide both global and local information. Accordingly we develop a low-complexity successive interference cancellation (SIC) algorithm to ILI and inter-cell interference (ICI) in the HM based SFN. The performance evaluation and decoding complexity comparisons indicate that the proposed structured SIC approach offers a good performance-complexity trade-off, especially for the HM-based SFN scenarios.

Finally, a BDR prototype has been developed on a personal computer (PC) based software defined radio (SDR) platform. Numerical results and initial laboratory tests demonstrate significant performance advantages of the new design over existing systems such as the Digital Radio Mondiale (DRM) and Hybrid Digital (HD) radio.

TABLE OF CONTENTS

Page

LIST OF FIGURES

LIST OF TABLES

ACKNOWLEDGMENTS

First and foremost, I would like to express my sincere gratitude to my advisor, Professor Hui Liu, for his professional advice and guidance throughout my studies at University of Washington. It has been a privilege, as well as great pleasure, to have the opportunity working closely with him. I have benefit a lot from his unique view of wireless communications and his ability to penetrate through the surface of complicated engineering problems to grasp the essence. He has greatly shaped my way of conducting research and tackling engineering problems. The experiences in the Wireless Information Technology Laboratory (WIT) under Professor Hui Liu are the most valuable times in my career and life. Besides this, he spent a lot of time on discussing research details with me, and reviewing my paper. I really learned a lot from Professor Hui Liu these years. If I had a chance to restart my Ph.D. life, I would definitely want to be his student again.

I would like to sincerely appreciate my thesis committee members, Professor Sumit Roy, Professor Payman Arabshahi and Professor Fei xia. Their valuable remarks and comments have made significant contributions to improving the quality of my dissertation. I am also grateful to Professor Jenq-Neng Hwang, Professor. James Ritcey, Professor. Radha Poovendran and all other professors, from whom I have learned a lot during my studies at University of Washington.

Many of my fellow students and colleagues gave me a lot of help on my research and life. Special thanks to my WIT lab colleague -Dr. Zhiyong Chen, thanks the two-year study and living experience with him. Although we have different personalities, it does not prevent us from being the best friends for ever. Also he is the most hardworking guy I have ever met, his passion for research always encourages me. Also I would like to my colleague Dr. Xun Shao, it is a valuable experience to work with him on the digital radio broadcasting project, I really learned a lot hands-on experience from him. I still can clearly remember the days

and nights we worked together on the project during the 2011 winter. When our designed prototype broadcasted the sweet music after 9 months hard work, we enjoyed the excitement and great achievement of success together at the moment. I would also like to thank my past and present colleagues at University of Washington, including Dr. Guanbin Xing, Dr. Han Huang, Wei Shi, Xiang Zou, Linda Bai, Yue yang, Dr. Ling Luo, Dr. Xiaofan Li, Min Sun, etc. Their collaboration and friendship make the pursuit of this degree more colorful and joyful.

Finally, I would like to be very grateful to my parents Yan Hu, Meizhen Wang, and my lovely wife, Zhuxiu Chu. They are always the constant source of love and support. Without their unconditional support, patience, and sacrifice, I could have never made it this far. They will always have my love. To them, I dedicate this dissertation.

Chapter 1

INTRODUCTION

1.1 Digital Radio Broadcasting

Due to inadequate spectrum resources and increasing demands for high quality multimedia services, traditional analog audio broadcasting is being migrated into digital radio around the world. A number of digital audio broadcasting standards have been developed in recent years, such as Digital Audio Broadcasting (DAB and DAB+; worldwide), Digital Multimedia Broadcasting (DMB; worldwide) and Integrated Services Digital Broadcasting (ISDB; Japan), etc. A comprehensive survey can be found in [1][2]. Among them, the Digital Radio Mondiale (DRM) [3] and the NRSC-5 standardized by the National Radio Systems Committee (NRSC)* are the most prominent ones. In addition, NRSC-5 is termed "in-band on-channel (IBOC)" in reference to the fact that digital and analog radio signals can co-exist in the same part of the spectrum. The IBOC technologies provide an uninterrupted evolution path from analog amplitude modulation (AM) and frequency modulation (FM) radio to a fully digital radio broadcasting system. The evolution allows listeners to migrate to digital reception of their favorite analog stations with IBOC capability. The history and state of the art of IBOC technologies are well documented in the book by Maxson [4]. In additional to the deploymental advantage, the IBOC digital radio can provide near Compact Disc (CD) sound quality as well as multi-media services such as data, image and even video.

The co-existence of digital and analog radio on AM and FM bands poses a few unique challenges on the design of digital broadcasting systems. First of all, inserting digital radio broadcasting into the established analog radio spectrum may cause interference to existing stations. Therefore, the digital signal power should be much lower (more than 20 dB power down is recommended, see [3]) than that of the analog signal, resulting in tolerable

*See http://www.nrscstandards.org/

interference on the analog signal reception. On the other hand, due to the huge power level difference, the use of low power digital radio technology with strong resistance to analog interference is a design mandate. Secondly, gaps between existing analog radio bands are fragmental in most cases. An ideal digital radio system must possess the spectrum efficiency and flexibility to offer high data rates without the use of a large amount of continuous bandwidth. Thirdly, the available FM/AM spectra for digital transmission are narrowband in nature. It is well documented that in wireless communications, stationary and low mobility users are likely to suffer from prolonged poor reception due to the lack of frequency diversity. Such a phenomenon is particularly evident in digital broadcasting as its performance degradation tends to be much more rapid than that of analog broadcasting. While both the DRM and the NRSC-5 effectively tackle the co-channel problem with suites of innovations, neither adequately address the data rate (e.g., DRM only supports the net data rate from 37.3 to 149.1kpbs, while the new broadband digital radio system described in this dissertation can support a net data rate from 35 kbps to 2.53 Mbps) and the fading performance issues (e.g. Long interleaving is applied in DRM and NRSC-5, however it may not be sufficient against slow fading cases).

1.2 Broadband Digital Radio System

In collaboration with SARFT[†] of China, we have developed a suite of innovative digital broadcasting technologies, and more importantly, a broadband digital broadcasting specification that meets and exceeds the specific set of requirements in IBOC broadcasting. According to the SARFT requirements, the new digital broadcasting system should offer: (1) better and richer user experiences than the traditional analog broadcasting with smaller bandwidth; (2) compatibility/coexistence with existing analog radio stations; (3) more multimedia features specifically for the Chinese market (e.g., audio/video reception in the high-speed vehicle, audio sideshows with image and animation); (4) bandwidth flexibility from 100 KHz up to 800 KHz. This newly developed specification has a promising marketing prospect in China and is scheduled in commercial trials in the major cities (e.g., Shanghai,

[†]State Administration of Radio, Film, and Television of China

Guangzhou, etc) by early 2013. Currently, there are approximately 2338 television and radio broadcasting stations in China, which constitutes one of the largest broadcasting networks in the world. The audio audience accounts for 96.31 percent of the population, with a total of 500 million radio receivers. If all the radio equipment are converted to the digital terminals, the market value can reach 1 billion dollars (assuming 20 dollars per equipment on average). In addition, more than 40 million automotive radio equipment need to be migrated into digital equipment, which can potentially lead to a 3.5 billion dollars market.

The salient features of the newly designed Broadband Digital Radio (BDR) specification include:

- capacity approaching irregular Low Density Parity Check (LDPC) codes for better interference resistance and higher receiver sensitivity;

- Orthogonal frequency-division multiplexing (OFDM) based band aggregation for high data rate broadcasting up to 2.53 Mbps, allowing multiple audio/video programs to be delivered along with audio services;

- frequency hopping for frequency diversity in slow fading/interference channels. The gain is particularly significant in stationary and pedestrian applications;

- novel hierarchical modulation schemes (2.5 - 5 dB better than that used in DVB-T) for layered audio and video broadcasting services.

1.3 Outlines

The dissertation is organized as the following. A system overview is provided in Chapter 2, along with the design philosophy and technical description of the BDR system. The new design synergistically integrates frequency hopping, low-density parity-check (LDPC) coding, hierarchical modulation and band aggregation techniques to increase the data rate, improve spectrum efficiency, and at the same time, provide the spectrum flexibility necessary in high quality audio and multimedia services.

One of the key design features in BDR is the powerful hierarchical modulation scheme that offers significant performance enhancement over existing schemes (e.g., DVB-T). In Chapter 3, we present a novel decoding algorithm for the hierarchical modulation in the BDR. Unlike the traditional hierarchical demodulation approaches which suffer from serious inter-layer interference (ILI), the proposed method exploits the structure information of the secondary layer to mitigate the ILI impairment, thereby offers significant gains in reception performance. The algorithm can be applied to different channel coding and mappings schemes under various channel profiles. Also included in the chapter is a computational complexity analysis, which reveals that the structure-based decoding approach achieves an excellent performance-complexity trade-off in the HM scenario. In addition, the HM achievable rate is analyzed by calculating the theoretical limit of the basic layer in HM reception, which in certain cases, is 6 dB better than the required signal-to-noise-plus-interference ratio (SINR) threshold for QAM detection with all Gaussian interference. Numerical results from both simulations and experiments are provided to quantify the performance advantages of the new algorithm against the digital video broadcasting-terrestrial (DVB-T) benchmark.

For the digital network, frequency planning is needed as in other digital broadcasting signals. Most importantly, the single frequency network (SFN) architecture will be used in the BDR deployment. In Chapter 4, the hierarchical modulation (HM) technique is adopted in a single frequency network (SFN) to provide both global and local information. Accordingly we develop a low-complexity successive interference cancellation (SIC) algorithm to mitigate the inter-layer interference (ILI) and inter-cell interference (ICI) in the HM based SFN. The performance evaluation and decoding complexity comparisons indicate that the proposed structured SIC approach offers a good performance-complexity trade-off, especially for the HM-based SFN scenarios.

Chapter 5 provides the performance evaluation of the BDR system. Also we move to the development aspect of my Ph. D work, the BDR prototype on the PC-based software defined radio (SDR) and some initial lab test results are presented.

Finally in Chapter 6, the research topics for future work are presented.

Chapter 2

ENABLING TECHNOLOGIES FOR BROADBAND IN-BAND ON-CHANNEL DIGITAL RADIO

In this chapter, we will provide the system overview, design philosophy and innovative broadcasting technologies for the Broadband Digital Radio (BDR) system.

2.1 System Specifications

2.1.1 Overview

As is required in all IBOC systems, the digital Broadband Digital Radio (BDR) channels must co-exist with existing analog FM channels, as shown in Fig. 2.1. This is possible due to the fact that digital broadcasting can reach the same coverage as analog broadcasting with much lower transmission power. Typically, the transmission power of BDR is above 20 dB lower than that of FM for comparable coverage.

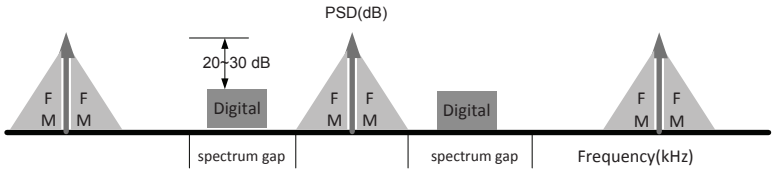

Figure 2.1: Digital Radio channels co-exist with existing analog FM channels

The BDR in FM band is designed to broadcast in the VHF band up to 108 MHz. At the physical layer, each BDR channel occupies 100 kHz bandwidth and is placed in a grid of 50 kHz, as shown in Fig. 2.3. The baseband transmission is based on OFDM, which provides the spectrum efficiency and scalability needed in initial deployment. The modulation schemes supported include QPSK, 16-QAM and 64-QAM, with both uniform and non-uniform constellations (depending on whether hierarchical modulation is enabled -

see more details in Section 2.1.6). Other key parameters of BDR are summarized in Table 2.1.

Table 2.1: System parameters

Parameter	Symbol	Value
Single band bandwidth	B	96.6 kHz
Subcarrier spacing	Δf	468.75 Hz
Number of subcarrier	N_{sc}	206
Symbol duration (data)	T_u	2.1333 ms
Guard interval duration	T_g	24.167 μs
Symbol duration	T_s	2.375 ms
Time slot duration	T_{ts}	80.75 ms
Frame duration	T_f	650 ms
Channel coding		LDPC
Code rate	r	$\frac{1}{4}, \frac{1}{3}, \frac{1}{2}, \frac{3}{4}$
Single band Data rate	R	35.4 - 319.0 kbps
Max aggregated data rate	Ra,max	2.552 Mbps

With different combinations of modulation and channel coding rates, a single 100 kHz BDR band can support a net data rate between 35 to 319 kbps. Multiple high quality audio programs, data services, and even video programs can be broadcasted in one BDR band. Fig. 2.2 exemplifies a BDR simulcast scenario with two audio programs and some data services.

One of the unique features of BDR is its capability to aggregate multiple bands to form a wider service channel for higher data rate broadcasting. In particular, band aggregation is supported in the range of $\pm$400 kHz around the hosting FM carrier. This aggregation option provides the flexibility to manage the fragmental gaps in analog radio broadcasting spectra. Fig. 2.3 illustrates the idea of band aggregation. In this particular example, the use of

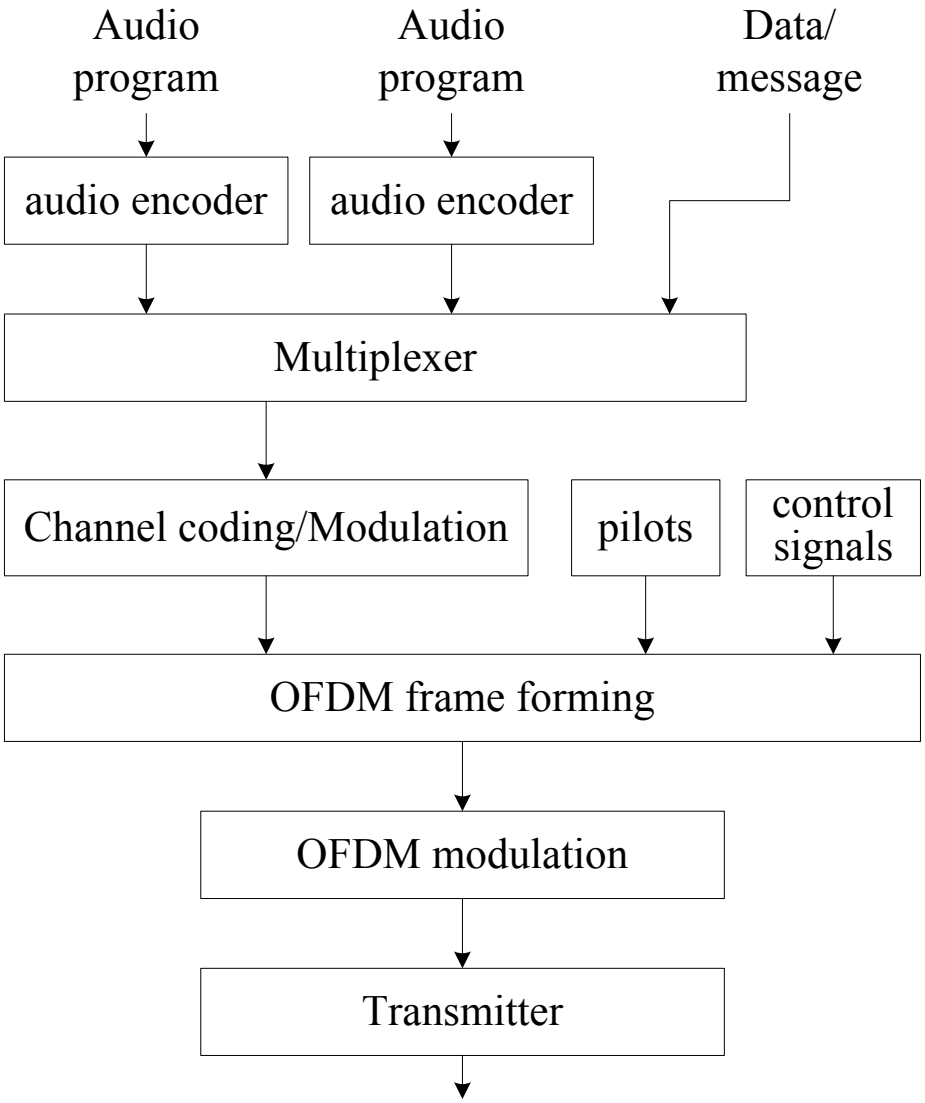

Figure 2.2: Block diagram of an BDR system

band aggregation results to a total bandwidth of 400 kHz and a maximum aggregated data rate of 1.276 Mbps. In the BDR design, up to eight bands (this option is not mandatory) can be aggregated in all digital transmission modes, yielding a maximum aggregated data rate of 2.53 Mbps. BDR can offer the bandwidth flexibility from 100 KHz up to 800 KHz, depending on the data rate requirements, channel availability, and market traction, etc.

When the bandwidth reduces to the 100 KHz, BDR has the similar frequency planning as DRM, while offering improved receiver sensitivity (see Chapter 5).

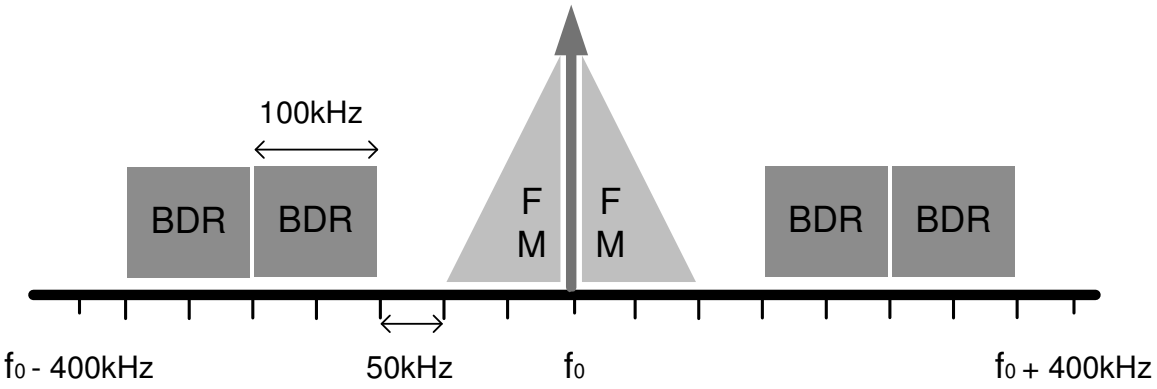

Figure 2.3: Spectrum allocation of FM BDR

2.1.2 Frame Structure

Fig. 2.4 depicts the frame structure of BDR. A number of factors are considered in determining the frame structure:

1. Fast synchronization: given the volatility of wireless channels, the BDR system must have the robustness to cope with fast and deep fading or even lost of signals over an extended period of time. When the radio link is interrupted, the receiver must be able to rapidly recover the system timing and frequency without going through the lengthy initiation process.

2. Frequency hopping: frequency hopping induced frequency diversity is essential in combating slow fading. Since the switching time of synthesizers varies, adequate time should be allocated to allow time-slot-by-time-slot frequency changes.

3. Granularity and power saving: in broadband broadcasting, a particular service program may only occupy a small fraction of the total data pipe. Ideally, the receiver

power consumption should be proportional to the program (i.e., the data rate) subscribed by the user. Fine granularity and power saving mechanisms are of fundamental importance in rich media applications.

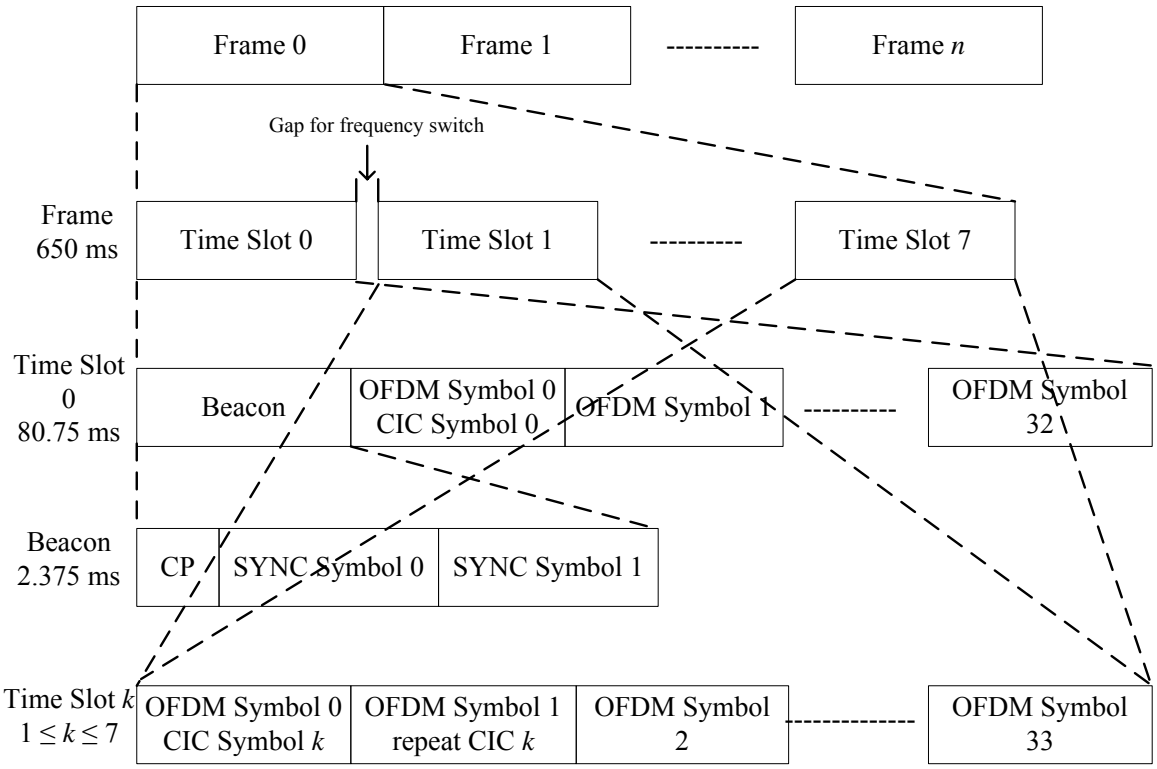

Figure 2.4: Frame structure

To accommodate the above requirements, the radio source is partitioned into frames of 650 ms duration. Each frame is divided into 8 time slots. The first time slot starts with a *beacon* followed by 33 OFDM symbols. The rest of the time slots are composed of 34 OFDM symbols each. The duration of a time slot is 80.75 ms. The beacon contains two identical band-limited pseudo random signals to facilitate time/frequency acquisition. In most cases, the receiver can achieve both timing and frequency synchronization based on a single beacon signal alone, indicating that the starting and recovering times of the BDR can be bounded within 650ms in theory. The gap between two consecutive time slots is

so designed to support frequency hopping. Details pertaining to frequency hopping will be described in Section 2.1.4.

Under the above setting, the granularity of the BDR is 35.1 kbps. Assuming that an audio program with FM-comparable sound quality consumes 35.1 kbps and a video program consumes 250 kbps, the basic BDR channel can support up to 8 audio programs or 1 video program with 2 audio programs simultaneously.

2.1.3 Signal Types

As shown in Fig. 2.5, three types of signals, namely, the *continuous pilots*, the *scattered pilots* and the *data signals*, are transmitted over the OFDM time-frequency grid. The continuous pilots mainly serve the purpose of frequency synchronization and phase tracking. In addition, the continuous pilots carry heavily protected *system information* such as the central frequency of the next time slot, information of the adaptive channel coding/modulation scheme and the interleaver, and a brief description of the programs carried. The system information bits repeat every time slot, and are QPSK modulated and protected with a Reed-Muller (RM) code.

Specifically, a second order (256, 16) RM code is employed to map 16 system information bits to a 256 bits code word as shown in Fig. 2.6. The output code word is a linear combination of 16 base sequences. The second order code is extended from a first order (256, 9) RM code. The first order RM code is equivalent to Hadamard code since its generation matrix is constructed from Hadamard matrices. To extend to the second order (256, 16) code, 7 mask sequences are selected. The mask sequences are derived from the Gold codes for their large minimum distance. The minimum distance of the (256, 16) code is 112. Finally, three (256,16) codewords are concatenated to carry 48 system information bits. At the decoder, fast Hadamard transform (FHT) can be applied to accelerate the decoding.

The rectangularly distributed scattered pilots are transmitted using known symbols and serve as a reference for channel estimation. The data signals occupy the rest of the time-frequency grid. The first OFDM symbol of each time slot carries *control information* -

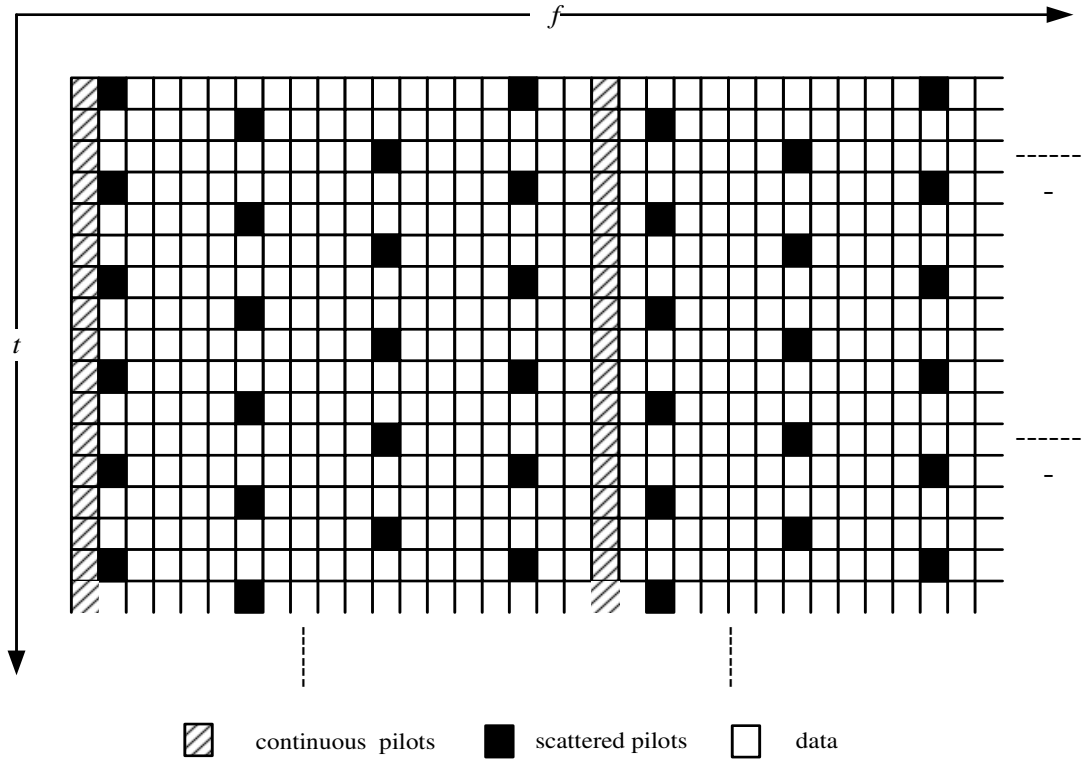

Figure 2.5: Signal types in time-frequency grid

eight of them within one frame are combined into a Control Information Channel (CIC) which contains the detailed control message of the broadcasting system. The power of the continuous pilots and the scattered pilots are boosted to be 3 dB higher than the data signals to provide extra robustness against fading.

2.1.4 Frequency Hopping

The typical coherent bandwidth in wide area applications is more than 1 MHz. Therefore, even with aggregation, the IBOC is a relatively narrow band system and does not possess sufficient frequency diversity in a fading environment. As a result, its performance is particularly poor for stationary and low mobility receivers where limited time domain diversity can be explored. In order to improve the performance, a frequency hopping option is adopted in BDR to introduce frequency diversity into the system. Fig. 2.7 illustrates the frequency

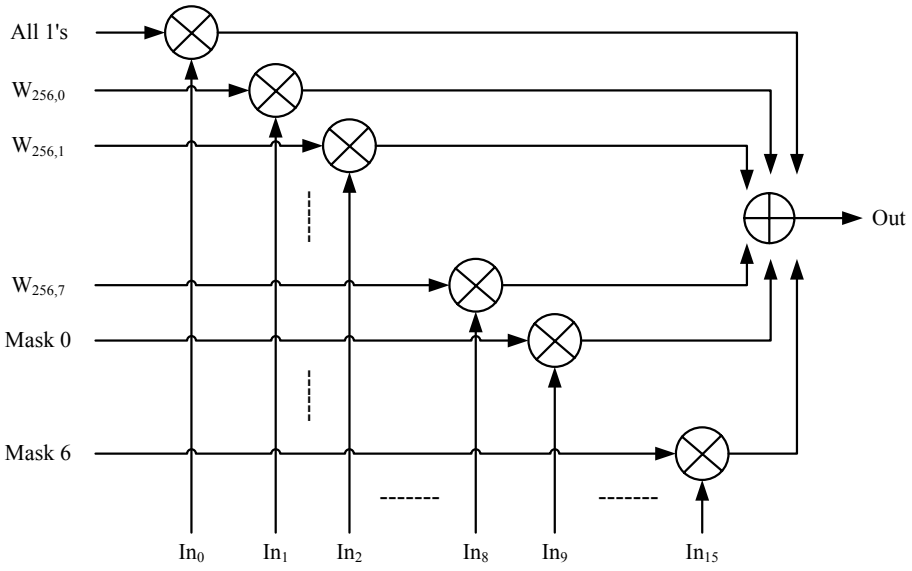

Figure 2.6: Encoder structure of Reed Muller code

hopping mechanism in BDR. In this example, a radio station has access to 4 bands. Without frequency hopping, each of the four band transmits one stream of programs, and the four streams are transmitted without coordination. When frequency hopping is applied, the transmission of the four streams is patterned by the station in time and frequency so that there is no conflicts or interference among streams. Specifically, each stream changes frequency every time slot and hops across 4 bands. The receivers acquire the frequency hopping sequence by decoding the continuous pilots of each time slot, which carries the central frequency of the next time slot. The efficacy of the frequency hopping against slow fading is quantified in Chapter 5.

2.1.5 LDPC code

LDPC codes are widely adopted in nowadays wireless communication standards for its Shannon-limit approaching performance and its inherent parallel structure for fast decoding [9]. In BDR, the irregular LDPC codes are modified based on the regular LDPC codes defined in the China Mobile Multimedia Broadcasting (CMMB) [33]. CMMB is a mobile television and multimedia broadcasting system developed by SARFT in 2006. The system

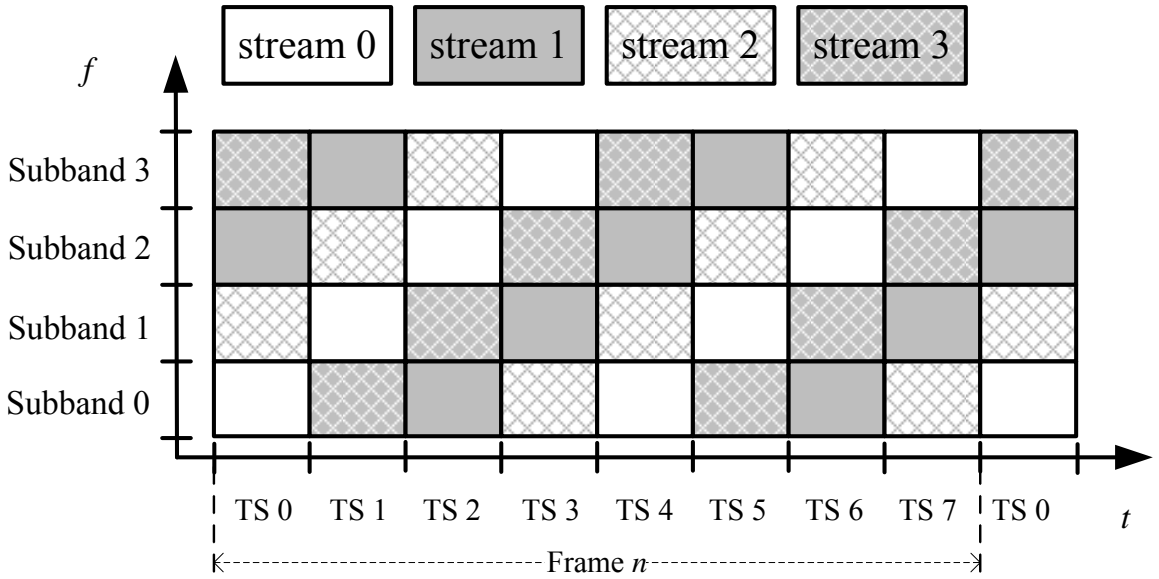

Figure 2.7: Example of frequency hopping

has been deployed in more than 300 cities with coverage reaching one billion population. The code length of the BDR LDPC is 9216 bits, which is the same as that of CMMB LDPC codes. Code rates of 1/4, 1/3, 1/2 and 3/4 are supported. Compared with the regular CMMB LDPC codes, the irregular BDR LDPC codes can provide 0.3 - 0.5 dB Eb/No (the energy per bit to noise power spectral density ratio) gain for different code rates. By modifying the LDPC codes from an established standard, BDR will offer the potential frame compatibility for the multi-mode terminals and benefit from a matured eco-system with large number of vendor supports.

2.1.6 Hierarchical modulation

Instead of the traditional single mode broadcasting, a hierarchical modulation scheme is adopted to further enrich the BDR services [32]. The basic idea of hierarchical broadcasting is to provide layered services to mobile users within different coverage areas, all through the same radio channel. For example, in a QPSK + QPSK hierarchical modulation mode, the broadcasting tower transmits non-uniform 16QAM audio signals (e.g., two layers of

QPSK signals set at different power levels) to all wireless terminals in the covered area. In this chapter, we will use the term *basic layer* signal to describe the essential data media transmission (e.g., the normal quality audio/video service); the enhancement information that is added on top of the basic layer will be named the *secondary layer* signal, which improves the media service quality. A user experiencing weaker signals (e.g., far from the transmitter) can only reliably demodulate the two bits QPSK signal of the basic layer, thus receives the normal quality audio service. When the signal strength becomes stronger, the user can potentially decode both layers of streams with a sum rate of four bits - the additional two bits in the secondary layer either represents another program, or simply enhances the audio service, providing near Compact Disc (CD) sound quality. When combined with scalable video coding (SVC) techniques [19], hierarchical broadcasting offers an appealing solution to the terminals with different screen sizes and different resolutions of video display.

It must be pointed out that the aforementioned advantages of hierarchical broadcasting does not come without a cost. Most noticeably, the added layer not only reduces the effective transmission power from the basic layer, but also incurs an additional performance loss to the basic layer reception. The prime cause of the degradation is the serious inter-layer interference (ILI). For example, in a two-layer QPSK+QPSK HM system, the C/N reception threshold of the basic layer is several dB (depending on the coding scheme) higher than that of the regular QPSK signal due to the fact that the secondary layer signal constitutes an interference to the basic layer. To minimize the performance loss, a number of different approaches have been proposed to mitigate the ILI impairments, e.g., the constellation rotation approach at the transmitter end, and the iterative decoding at the receiver end.

For the BDR system, we have incorporated a powerful hierarchical modulation scheme that offers significant performance enhancement over existing schemes (e.g., DVB-T). In particular, we have developed an LDPC decoding algorithm for the coded hierarchical demodulation signals, in which the LDPC decoder is refined to account for the non-Gaussian interference from the second layer [13]. The method greatly enhances the performance of hierarchical modulation in both AWGN and fading channels over DVB-T system. More details on the performance gains are provided in Chapter 5.

2.2 Conclusions

A Broadband Digital Radio system has been designed to meet the service requirements of next generation in-band on-channel digital radio broadcasting. By synergistically combining the LDPC codes, the band aggregation and the frequency hopping techniques, as well as an efficient hierarchical modulation scheme, BDR offers both performance and services advantages in various application scenarios. On the service side, the BDR supports a wide range of data rate (up to 2.53 Mbps) and is capable of delivering high quality radio and rich multi-media services such as data, image and video.

Chapter 3

A NOVEL LDPC DECODING ALGORITHM FOR HIERARCHICAL QAM MODULATION

As described in Chapter 2, the BDR system incorporated a powerful hierarchical modulation scheme that offers significant performance enhancement over existing schemes (e.g., DVB-T). At the receiver end we have developed a novel LDPC decoding algorithm for the coded hierarchical demodulation signals, in which the LDPC decoder is refined to account for the non-Gaussian interference from the second layer. In this chapter, we present a structure-based decoding algorithm for the BDR in detail. This decoding algorithm can be applied to different channel coding and mappings schemes under various channel profiles. Also included in the chapter is a computational complexity analysis, which reveals that the structure-based decoding approach achieves an excellent performance-complexity trade-off in the HM scenario. In addition, the HM achievable rate is analyzed by calculating the theoretical limit of the basic layer in HM reception, which in certain cases, is 6 dB better than the required signal-to-noise-plus-interference ratio (SINR) threshold for QAM detection with all Gaussian interference.

3.1 Background on Hierarchical Modulation

The increasing demand for high quality contents has driven the broadcasting industry to migrate from analog to digital transmission. To deliver more information through a fixed amount of bandwidth, high order modulation such as the 64-QAM has been adopted in wireless broadcasting systems (e.g., the DVB-T2) [14]. The incorporation of higher dimensional modulation inevitably leads to a much increased carrier to noise ratio (C/N) threshold for reception, resulting in a reduced coverage area relative to more robust modulation schemes. To balance the data rate and the coverage area, hierarchical modulation (HM) based transmission schemes [16]-[18] have been introduced to offer graceful tradeoffs between the C/N reception threshold and the amount of information a terminal can receive. Unlike the tra-

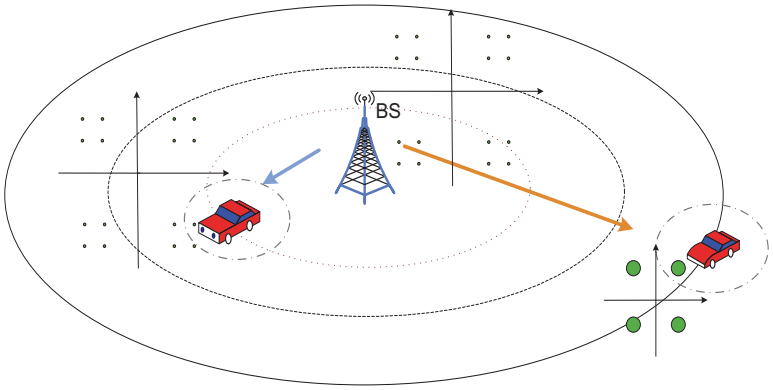

Figure 3.1: Hierarchical QAM modulation for different coverage (QPSK+QPSK case).

ditional single-layer broadcasting, the HM broadcasting system provides multiple layers of data streams, each of which has a different C/N threshold and a corresponding coverage area, all within the same transmission bandwidth.

Fig. 3.1 illustrates a QPSK+QPSK HM system where two layers of QPSK signals are superimposed before broadcasting (detailed block diagram of HM encoder can refer to Fig. 3.2). In this particular case, the broadcast station (BS) transmits non-uniform 16QAM audio signals (e.g., two layers of QPSK signals set at different power levels) to all wireless terminals in the covered area. In this chapter, we will use the term *basic layer* signal to describe the essential data media transmission (e.g., the normal quality audio/video service); the enhancement information that is added on top of the basic layer will be named the *secondary layer* signal, which improves the media service quality. As can be observed from Fig. 3.1, a terminal far from the BS may only be able to reliably demodulate the 2-bit QPSK signal of the basic layer, thus receives a normal quality audio service. On the other hand, a terminal with high C/N value could potentially decode both the basic layer and the secondary layer with a sum rate of four bits. The additional two bits in the secondary layer could be used to enhance the audio/video services. When combined with scalable video coding (SVC) techniques [19][20], hierarchical broadcasting offers an appealing solution to the terminals with different screen sizes and different resolutions of video display.

It must be pointed out that the aforementioned advantages of hierarchical broadcasting

does not come without a cost. Most noticeably, the added layer not only reduces the effective transmission power from the basic layer, but also incurs an additional performance loss to the basic layer reception. The prime cause of the degradation is the serious inter-layer interference (ILI). For example, in a two-layer QPSK+QPSK HM system, the C/N reception threshold of the basic layer is several dB (depending on the coding scheme) higher than that of the regular QPSK signal due to the fact that the secondary layer signal constitutes an interference to the basic layer.

The penalty of ILI in the HM scheme has been well analyzed [32]. A number of different approaches have been proposed to mitigate its impairments. These approaches can be classified into two categories: ILI mitigation approaches at the transmitter end [21]-[23], and ILI mitigation approaches at the receiver end [24]-[27].

The ILI mitigation approaches at the transmitter end focus on the constellations design and pre-coding techniques. In particular, the constellation rotation approach has been presented in [21], which judiciously rotates the secondary layer signal constellation to improve the basic layer achievable rate. A more general approach was proposed in [22], which designs a new non-uniform QAM constellation to reduce the performance loss in the basic layer. However, the performance gains offered by both approaches become limited when the HM signals are channel coded (e.g., LPDC, Turbo code), which restricts its applicability. Another pre-coding approach has been proposed in [23], which utilizes the dirty paper coding (DPC) technique to reduce the ILI in the HM transmission. However this approach cannot be easily applied to the fading channels, since DPC technique is very sensitive to the channel estimation errors. Furthermore, this approach only considers the QPSK+QPSK HM case in the paper, the extension to other larger constellations (e.g., QPSK+16QAM) is not straightforward.

Without a computational constraint, the basic layer reception can be improved at the receiver end by using multi-layer iterative decoding/successive cancellation, in which all layers are decoded even though the only signal of interest is the basic layer. In [24], a new turbo iteration algorithm was introduced in the HM based OFDM system. Similarly, an iterative frequency-domain turbo receivers was proposed in the single-carrier with frequency-domain equalization (SC-FDE) scheme [25] with HM. However the decoding complexity of both ap-

proaches can be extremely high. In [26][27], an iterative receiver was designed for the joint detection and channel estimation for the wideband code division multiple access (WCDMA) systems with hierarchical constellations, the performance gain is mainly attributed to interference suppression and enhanced channel estimation in WCDMA. Despite of their effectiveness, all the aforementioned iterative approaches suffer from one or more of the following limitations in HM reception: (1) The decoding complexity/delay of the multi-layer iterative decoding approach is high due to the large number of iterations and the Log-likelihood ratio (LLR) computations for signals of all layers, especially when the HM constellation is high (e.g., QPSK+16QAM). A low-complexity decoding strategy is highly desirable for the HM signal detection; (2) The number of outside iterations (iterations between the demodulator and channel decoder) and inner iterations (iterations inside the channel decoder) must be tuned in order to achieve the best performance. This could be problematic with changing signal-to-noise-plus-interference ratio (SINR) values and channel characteristics; (3) The multi-layer iterative decoding does not work well when the HM signal have a strong basic layer signal and a relatively weak secondary layer signal. As a matter of fact, the relatively weak secondary layer signal cannot offer much gain for the basic layer detection during the iterations, especially in the low SINR region. Among the three issues, the first two limitations are particularly important in the real system implementation.

Given that channel coding is a performance mandate in most wireless systems, great importance should be attached to improving the performance of the coded HM systems [24]-[28]. Towards this end, we examine the channel coded HM signals and attempt to design a low-complexity demodulation/decoding algorithm, which can practically address the performance loss caused by the QAM-structured ILI directly at the receiver end. Specifically, we notice that the non-Gaussian structure of QAM interference has not been sufficiently exploited in the decoding algorithm. This observation motivates us to develop a high performance decoding strategy that incorporates the *secondary layer structure* in the HM demodulation/decoding. In the following, we consider an LDPC coded HM system and investigate the demodulation/decoding scheme for the basic layer signal. The LDPC decoder introduced in [35] will be used in conjunction with the structure-based soft-input-soft-output (SISO) detector to improve the interference resistance. The main contributions

of this work include the following.

1. Development of a basic layer decoding algorithm which treats the statistics of the secondary layer signals as the side information. The new decoding algorithm can effectively mitigate the ILI inherited in the hierarchical demodulation. Thanks to the refined metric for the LLR calculation and an optimized mapping rule for the HM constellations, the decoding algorithm can be applied to different soft-decision channel coding schemes (e.g., LPDC, Turbo code; in this chapter we assume LDPC as the coding choice) and mapping schemes under various channel profiles. Also the proposed algorithm can be easily implemented on both single-carrier systems (e.g., single-carrier FDMA) and multi-carrier systems (e.g., OFDM).

2. Computational complexity analysis on the proposed decoding algorithm. By comparing the performance of a few decoding approaches, we show that the proposed structure-based decoding algorithm offers a good performance-complexity trade-off in the HM scenario.

3. Achievable rate derivation and performance analysis on the QAM-based HM scheme. Our results establish a theoretical bound for the basic layer signal reception. Simulations show that the structure-based decoding algorithm can offer up to 6 dB gain over the required SINR value for the QAM detection when the power ratio (defined in Section 3.2) goes to infinity.

4. Implementation of the proposed algorithm in a real-world OFDM-based broadband digital radio (BRD) system [34].

The rest of chapter is organized as follows. Section 3.2 presents the LDPC coded HM system and overviews of the traditional demodulation/decoding technique. Section 3.3 firstly puts forth the structure-based decoding algorithm for the basic layer, and then develops the constellations and mapping rules for the proposed decoding algorithm, finally the computational complexity analysis is provided. Section 3.4 presents the achievable rate derivation

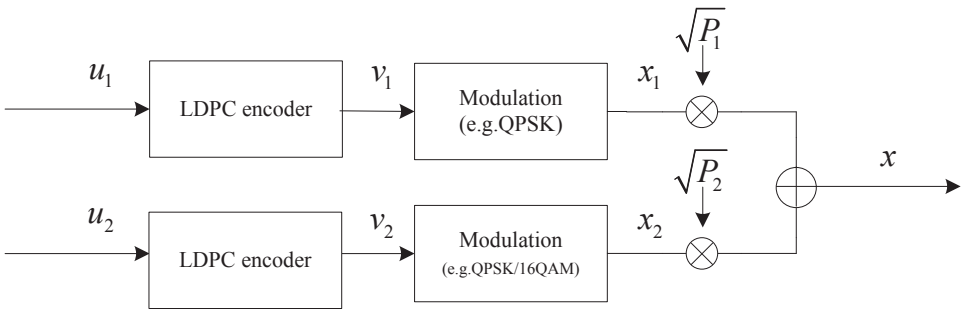

Figure 3.2: Transmitter structure of LDPC coded HM.

and analyzes the proposed algorithm. We evaluate the performance of the structure-based decoding algorithm in Section 3.5, and in Section 3.6 we describe the algorithm implementation on the BDR. Finally, a conclusion is drawn in Section 3.7.

3.2 System Model and Definitions

3.2.1 Coded HM signals

In theory, multiple layers of source information can be delivered to users experiencing different channel qualities through HM. In this chapter, only the two-layer HM transmission is investigated, which is sufficient for practical wireless systems (e.g., a QPSK+16QAM HM signal can provide the non-uniform 64QAM constellation). We denote the symbol alphabet $\mathbf{u}_i$ $(i = 1, 2)$ as the information bits for the basic layer and secondary layer, respectively. $\mathbf{v}_i$ denotes the corresponding coded bits after LDPC encoder: $\mathbf{v}_i = [v_i^1, ..., v_i^n]^T$, where v_i^n is the nth coded bit of layer i. The coded bits from each layer are then modulated into $\mathbf{x}_i$ using QAM, $\mathbf{x}_i = [x_i^1, ..., x_i^k]^T$, where x_i^k denotes the kth symbol of layer i.

Fig. 3.2 illustrates the transmitter structure of the LDPC coded HM. The two data streams $\mathbf{u}_i$ are independently coded using the LDPC encoders and then modulated using QAM with amplitude set to be $\sqrt{P_1}$ and $\sqrt{P_2}$, respectively. Finally, the symbols from the two layers are superimposed into $\mathbf{x}$ before transmission. Mathematically, the transmitted HM signal is given by

$$\mathbf{x} = \sqrt{P_1}\mathbf{x}_1 + \sqrt{P_2}\mathbf{x}_2, \tag{3.1}$$

with $P_1 + P_2 = P$, where P is total transmission power. More precisely, the secondary layer symbols $\mathbf{x}_2$ in Equation (3.1) should be written as $\mathbf{x}_2(\mathbf{x}_1)$ to emphasize its dependency on x1 (e.g., the Gray mapping [14][15]). Since the notation $\mathbf{x}_2$ does not affect our derivation of the decoding method,, we use $\mathbf{x}_2$ here for convenience.

Let λ be the power ratio between the basic layer signal and the secondary layer,

$$\lambda = \frac{P_1}{P_2}. \tag{3.2}$$

In the HM system, λ is an important parameter that determines the power allocation among the layers. In QAM HM, λ characterizes the constellation of hierarchical signals. For example, the QPSM+QPSK HM constellation becomes the uniform 16QAM when $\lambda = 6$ dB. In this chapter, we will limited our attention to the cases with $\lambda \geq 6$ dB, where the constellation is truly hierarchical. In the extreme case, e.g., $\lambda = \infty$, all the transmission power is assigned to the basic layer, HM signal essentially reduces to the single-layer constellation.

3.2.2 Traditional receiver for coded HM signals

At the receiver side, a user with low signal strength simply demodulates/decodes the basic information, whereas users with higher signal strength can demodulate/decode both the basic and the secondary layer information from the constellation. To explain the difference, note that the signal received at the user end is given by

$$\mathbf{y} = \sqrt{P}_1\mathbf{x}_1 + \sqrt{P}_2\mathbf{x}_2 + \mathbf{n}, \tag{3.3}$$

where $\mathbf{n}$ is the Gaussian noise vector at the receiver, assumed to be Gaussian with variance σ^2, $\mathbf{n} = [n_1, ..., n_k]^T$; $\mathbf{y}$ denotes the received symbol vector, $\mathbf{y} = [y_1, ..., y_k]^T$.

Before proceeding, we introduce the achievable rate notations used in the chapter hereafter in Table 3.1.

With independent demodulation/decoding, e.g., each layer treats the other layer as interference, the following rate pair is achievable [23]

$$R_b = B\log_2(1 + \frac{P_1}{P_2 + \sigma^2}), \tag{3.4}$$

Table 3.1: summary of notations

R_b	basic layer achievable rate in HM system
R_s	secondary layer achievable rate in HM system
$R_{s,succ}$	secondary layer achievable rate using successive decoding in HM system
$R_{b,sb}$	basic layer achievable rate using structure-based decoding in HM system

$$R_s = B\log_2(1+\frac{P_2}{P_1+\sigma^2}), \tag{3.5}$$

where B is the channel bandwidth. Clearly, the two modulated signals interfere with each other, leading to a certain performance loss at the receiver end. Note that, in the QAM based HM, the effective noise $\overline{\mathbf{n}} = \sqrt{P_2}\mathbf{x}_2 + \mathbf{n}$ for the basic layer is not Gaussian distributed.

For the secondary layer signal reception, successive decoding strategy can be employed firstly to decode $\mathbf{x}_1$ and then subtract it from the received signal $\mathbf{y}$. $\mathbf{x}_2$ can then be demodulated/decoded from the remaining signal. With such successive decoding, a larger achievable rate can be achieved for the secondary layer [23],

$$R_{s,succ} = B\log_2(1+\frac{P_2}{\sigma^2}). \tag{3.6}$$

3.3 Structure-based Decoding for the Basic Layer in HM system

As mentioned in Sections 3.1 and 3.2, demodulation of the basic layer signal in HM suffers from serious ILI caused by the secondary layer. A more efficient decoding scheme must be developed in order to approach or surpass the theoretical achievable rate R_b for the basic layer. In this section, we first present a structure-based decoding algorithm that takes advantage of the QAM structure of secondary layer signal as the side information. The new decoding algorithm can largely cancel out the ILI for the basic layer without undue complexity. Subsequently, we analyze the constellations and mapping rule for the proposed decoding algorithm. Finally the computational complexity analysis for different decoding

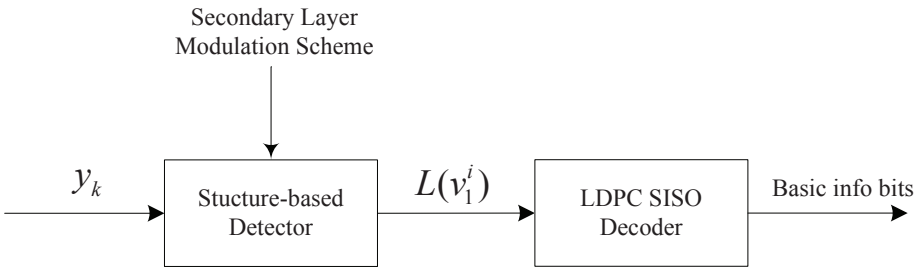

Figure 3.3: Block diagram of the structure-based decoder for the basic layer.

approaches is provided.

3.3.1 Structure-based Decoding

The structure-based decoder is motivated by the following observation. In QAM-based HM broadcasting, the modulation scheme of each layer (for basic and secondary information) is sent over a control channel. As a result, the QAM structure information* is available for the demodulation/decoding of both layers. In particular, as shown in Fig. 3.3, the receiver has prior knowledge of the secondary layer modulation scheme when demodulating/decoding the basic layer. This extra information can be used to modify the LLR of the basic layer coded bits (in traditional HM reception, the QAM demodulators simply calculates the LLR assuming the interference is Gaussian distributed, the resulting LLR is then fed into the LDPC decoder).

Accordingly, the new receiver for the basic layer is comprised of two parts: a structure-based detector which produces modified soft information in the form of LLR, and a SISO LDPC decoder that incorporates the LLR. The structure-based detector has two inputs, one of which is the second layer structure information while the other is the kth received symbol, which can be expressed as

$$y_k = \sqrt{P_1}x_1^k + \sqrt{P_2}x_2^k + n_k. \tag{3.7}$$

*In this chapter, we use the term "structure information" to refer to the modulation structure of the layers, e.g., QPSK, 16QAM.

Besides y_k, the modulation scheme and consequently the distribution function of x_2 is also know to the detector. In other words, the mapping from the l_2 information bits onto the kth symbol x_2^k in the secondary layer is known as the prior information: $(v_2^1, ..., v_2^{l_2})^k \rightarrow x_2^k$, where $(v_2^1, ..., v_2^{l_2})^k$ is the kth random vector that spans $\{0,1\}^{l_2}$. Based on the extra information, the bit level modified LLR expression can be derived as follows. First, we rewrite Equation (3.7) as

$$y_k = \sqrt{P_1} x_1^k(v_1^1, ..., v_1^{l_1}) + \sqrt{P_2} x_2^k(v_2^1, ..., v_2^{l_2}) + n_k. \tag{3.8}$$

Unlike the traditional QAM demodulators, which calculate the LLR only based on the observation y_k, the structure-based detector produces the refined LLR soft information by accounting for the mapping information (l_2 bits are mapped into a symbol) in the secondary layer.

For AWGN channels, the modified LLR value for the ith bit of x_1^k can be expressed as

$$\begin{aligned} L(v_1^i) &= \log \frac{P[v_1^i = 0 | y_k; \text{mapping information of } x_2^k]}{P[v_1^i = 1 | y_k; \text{mapping information of } x_2^k]} \\ &= \log \frac{\sum_{(v_2^1,...,v_2^{l_2}) \in \{0,1\}^{l_2}} P[v_1^i = 0 | y_k, v_2^1, ..., v_2^{l_2}] P(v_2^1, ..., v_2^{l_2})}{\sum_{(v_2^1,...,v_2^{l_2}) \in \{0,1\}^{l_2}} P[v_1^i = 1 | y_k, v_2^1, ..., v_2^{l_2}] P(v_2^1, ..., v_2^{l_2})} \\ &= \log \frac{\sum_{(v_2^1,...,v_2^{l_2}) \in \{0,1\}^{l_2}} \exp(-D(v_1^i = 0; v_2^1, ..., v_2^{l_2}))}{\sum_{(v_2^1,...,v_2^{l_2}) \in \{0,1\}^{l_2}} \exp(-D(v_1^i = 1; v_2^1, ..., v_2^{l_2}))}, \end{aligned} \tag{3.9}$$

where

$$\begin{aligned} D(v_1^i = 0; v_2^1, ..., v_2^{l_2}) &\doteq \tfrac{1}{2\sigma^2} || y_k - \sqrt{P_1} x_1^k(v_1^1, ... v_1^{i-1}, 0, v_1^{i+1}, ... v_1^{l_1}) - \sqrt{P_2} x_2^k(v_2^1, ..., v_2^{l_2}) ||^2 \\ D(v_1^i = 1; v_2^1, ..., v_2^{l_2}) &\doteq \tfrac{1}{2\sigma^2} || y_k - \sqrt{P_1} x_1^k(v_1^1, ... v_1^{i-1}, 1, v_1^{i+1}, ... v_1^{l_1}) - \sqrt{P_2} x_2^k(v_2^1, ..., v_2^{l_2}) ||^2. \end{aligned} \tag{3.10}$$

Since the secondary layer symbols x_2^k are independently and uniformly distributed on their own constellations, the term $P(v_2^1, ..., v_2^{l_2})$ can be cancelled out in Equation (3.9) which will reduce the number of multiplications in the LLR computation.

The structure-based detector can also be applied to different channel profiles (see Section

3.6). For fading channels, the kth received symbol can be expressed as

$$y_k = h_k(\sqrt{P_1}x_1^k + \sqrt{P_2}x_2^k) + n_k, \tag{3.11}$$

where h_k is the channel response for the kth transmitted symbol. The same LLR expression as Equation (3.9) still applies, except Equation (3.10) is adjusted to

$$D(v_1^i = 0; v_2^1, ..., v_2^{l_2}) \doteq \frac{1}{2\sigma^2}||y_k - h_k\sqrt{P_1}x_1^k(v_1^1, ...v_1^{i-1}, 0, v_1^{i+1}, ...v_1^{l_1}) - h_k\sqrt{P_2}x_2^k(v_2^1, ..., v_2^{l_2})||^2$$
$$D(v_1^i = 1; v_2^1, ..., v_2^{l_2}) \doteq \frac{1}{2\sigma^2}||y_k - h_k\sqrt{P_1}x_1^k(v_1^1, ...v_1^{i-1}, 1, v_1^{i+1}, ...v_1^{l_1}) - h_k\sqrt{P_2}x_2^k(v_2^1, ..., v_2^{l_2})||^2. \tag{3.12}$$

With the modified LLR expressions for different channel models, we are ready to pass them into the SISO LDPC decoder and start decoding iteration as follows [35]:

- *Initialization* **:** Given the received signal y_k and secondary layer structure, calculate the $L(v_1^i)$ for $i = 1, ..., l_1$ according to Equation (3.9). Set $L_{i\to j} = L_i = L(v_1^i)$.

- *Iteration* **:**

  - *Check node update* **:** compute outgoing check node messages $L_{j\to i}$ using Equation (3.13) and then pass them to the variable nodes.

$$L_{i\to j}^l = 2\tanh^{-1}\prod_{i'\in N\{j\}-\{i\}}\tanh(\frac{L_{i'\to j}}{2}), \tag{3.13}$$

    where $N(j)$ is the set of neighboring variable nodes to the jth check node.

  - *Variable node update* **:** compute outgoing variable node messages $L_{i\to j}$ using Equation (3.14) and then transmit them to the check nodes.

$$L_{i\to j} = L_i + \sum_{j'\in N\{i\}-\{j\}} L_{j'\to i}, \tag{3.14}$$

    where $N(i)$ is the set of neighboring check nodes to the ith variable node.

  - *LLR total* **:** For $i = 1, ..., n$ calculate

$$L_i^{total} = L_i + \sum_{j\in N(i)} L_{j\to i}. \tag{3.15}$$

– *Stopping criteria* **:** For $i = 1, ..., l_1$, estimate v_1^i from

$$\widehat{v_1^i} = \begin{cases} 1, & \text{if } L_i^{total} < 0, \\ 0, & \text{else,} \end{cases} \tag{3.16}$$

to obtain $\widehat{\mathbf{v}_1}.If\widehat{\mathbf{v}_1}\mathrm{H}^T = 0$ or the number of iterations equals the maximum limit, the algorithm stops; else go to the step of check node update.

3.3.2 Constellations and Mapping Rules

The structure-based decoding can be applied to different constellations and mappings (but not arbitrary), in this subsection we discuss the constellations and mapping rule for the proposed decoding approach.

In [15], the Gray mappings on the overall HM constellations (e.g, non-uniform 16QAM and non-uniform 64QAM) are proposed. An enhanced version named the *balanced hierarchical constellation* is introduced in [32], it also needs the constellations are entirely Gray mapped. The limitation of the overall Gray mapped HM constellations is that, the secondary layer mapping scheme should be dependent on the basic layer mapping scheme (e.g., if two independently Gray mapped QPSK signals are added together, the superposed 16QAM is no longer entire Gray mapped). Thus the entire Gray mapped HM constellations increase the complexity of modulation block in the hardware implementation, especially for large constellations. The constraint condition for mapping can be softened when adopting the structure-based coding, which only requires that each layer of the HM constellation is Gray mapped (the mappings for both layers are independent).

Take the QPSK+QPSK HM constellation for example. In Fig. 3.4(a) the overall non-uniform 16QAM constellation [32] is Gray mapped, and in Fig. 3.4(b) each layer of the HM constellation is Gray mapped (the overall constellation no longer maintains the Gray mapping). Let us look back on Equation (3.9), the basic layer LLR calculation is only related to: (1) basic layer mapping itself; (2) the values of all possible secondary layer symbols (four possible values in this example). Therefore the basic layer Gray mapping is enough to minimize the BER for the basic layer information bits, thus there is slightly difference between Fig. 3.4(a) and Fig. 3.4(b) when employing the structure-based decoding. If

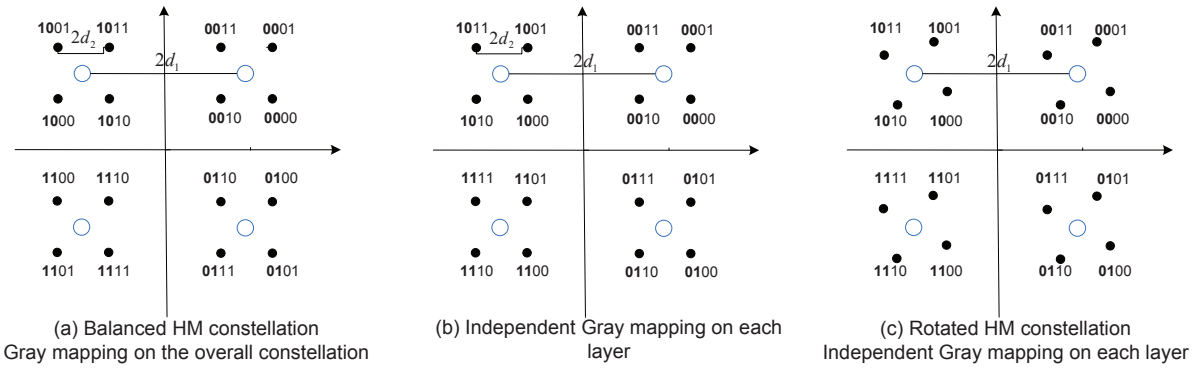

Figure 3.4: Different constellations and mappings for the QPSK+QPSK HM signal.

we want to further decode the secondary layer coded bits, usually the successive decoding strategy is applied. When correctly subtracting the already-detected basic layer signals from the received HM signals, the remained secondary layer constellations in both Fig. 3.4(a) and Fig. 3.4(b) are still Gray mapped. In a word, there is slight BER difference for the HM signal detection in both mapping schemes when using the structure-based decoding approach, but the mapping scheme in Fig. 3.4(b) is easier to implement and it reduces the mapping complexity. In addition, the structure-based decoding can also be applied to the rotated HM constellation as shown in Fig. 3.4(c), as long as it satisfies the mapping rule. Different designs of the rotated HM constellation are proposed in [21], which can be use to maximize spectral/modulation efficiency and minimize the peak-to-average-power ratio (PAPR) in the OFDM systems. When the rotated HM constellations are utilized in conjunction with the structure-based decoding, all the aforementioned advantages maintain, and at the same time the ILI is effectively mitigated.

3.3.3 Computational Complexity Analysis

In this subsection, we analyze the computational complexity of the structure-based decoding approach, and compare it with that of the multi-layer iterative decoding approaches.

The computation of the structure-based decoding approach mainly involves two parts, as can be observed from Fig. 3.3:

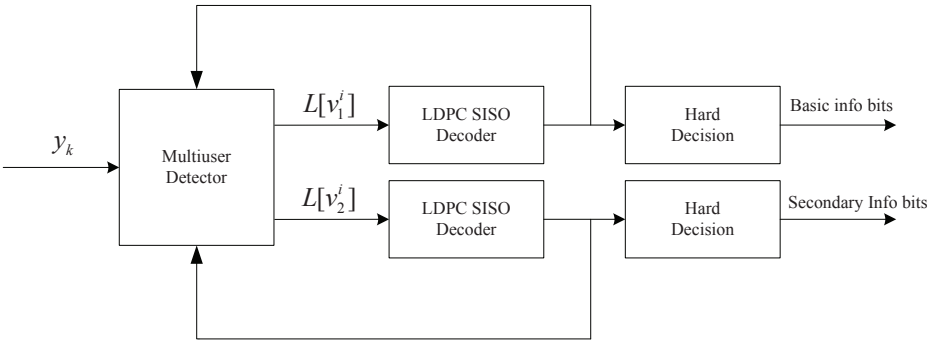

Figure 3.5: Block diagram of LDPC multi-layer iterative receiver.

- The LLR computation of the structure-based detector (SBD), which is based on Equation (3.9). The elimination of the term $P(v_2^1, ..., v_2^{l_2})$ greatly reduces the complexity.

- The iterations in the LDPC decoding, which are described from Equation (3.13) to Equation (3.16).

The block diagram of the LDPC multi-layer iterative decoding is shown in Fig. 3.5. The multiuser detector (MUD) outputs are connected to the soft inputs of two parallel LDPC decoders, which produce the extrinsic soft outputs (the extrinsic information calculations are not shown in Fig. 3.5). Then the soft outputs of these two decoders are fed back to the MUD, which can then improve its outputs along the iterations (the soft outputs of the two decoders are used to aid each other). After enough number of iterations, the outputs are forwarded to the hard decision block to generate the final information bits (the multi-layer iterative decoding details refer to [30][31]). The total computational complexity of the multi-layer iterative decoding approach is equal to the computational complexity of one iteration multiplying the number of iterations. For each iteration, the computational complexity mainly contains two parts as shown in Fig. 3.5:

- The LLR of the MUD, which delivers the *a posteriori* LLR of a transmitted "1" and a transmitted "0" for every code bit of every layer (Equation (4) in [31]).

- The iterations in the LDPC decoding, which are the same as those of structure-based decoding.

Before we compare the computational complexity of the structure-based decoding approach with that of the multi-layer iterative decoding approaches, some comparative prerequisites should be stated:

1. This chapter focuses on the ILI mitigation for the basic layer in HM. Hence for the multi-layer iterative decoding approach, only the basic layer computational complexity is counted. This prerequisite makes a fair complexity comparison between the structure-based decoding approach and the multi-layer iterative decoding approach.

2. The basic layer computation complexity of both approaches is compared in terms of the total number of: (1) operations on LLR computation; (2) the number of LDPC inner iterations for one LDPC block length. Keep in mind that the contribution for the number of operations on LLR computation is independent of its type, e.g., subtraction, multiplication, division, exponentiation and logarithm. In the case of complex operations, a complex multiplication is equivalent to four real multiplications plus two real additions, and each complex addition is equivalent to two real additions.

Table 3.2: Basic layer computational complexity comparison; QPSK+QPSK HM signal with independently Gray mapped CONSTELLATION; the number of outside iterations for the multi-layer iterative decoding $N_{out} = 5$; the number of LDPC decoder inner iterations $N_{in} = 40$; L denotes one LDPC block length.

	number of operations on LLR computation	number of LDPC inner iterations
Iterative decoding	$215L$	200
Structure-based decoding	$33L$	40
Computational saving	84.7%	80%

As an example we consider the basic layer computational complexity for QPSK+QPSK HM signal, the comparison results are summarized in Table 3.2. In this complexity evaluation table, the number of LDPC decoder inner iterations N_{in} is set to be 40 for both approaches, the number of outside iterations (between the LDPC decoder and MUD) N_{out} is set to be 5 for the multi-layer iterative decoding approach, L denotes one LDPC block length, each layer of the HM constellation is independently Gray mapped. As can be observed from Table 3.2, compared with the multi-layer iterative decoding approach, the structured-based decoding approach offers 84.7% computational saving on the LLR computation, and 84.7% saving on the number of LDPC decoder inner iterations. In section 3.5 we will show that, without decoding the secondary layers, the structure-based decoding approach still offers comparable basic layer BER performance with the multi-layer iterative decoding approach in the HM scenario. Such is particularly appearing to the HM signal, which is made up of a strong basic layer signal and a relatively weak secondary layer signal.

3.4 Basic layer achievable rate analysis

In this section, we analyze the basic layer achievable rate assuming the second layer structure information is incorporated in decoding.

Lemma 1 *With the structure information from the secondary layer, the basic layer achievable rate is upper bounded by* $R_{b,sb} = B\log_2(1+\frac{P_1}{\sigma^2})$.

Proof. *As mentioned in Section II, the basic layer achievable rate with traditional demodulation/decoding (e.g., without exploiting the second layer structure information) is* $R_b = B\log_2(1+\frac{P_1}{P_2+\sigma^2})$. *Under the most extreme case where the secondary layer interference is deterministic, the ILI can be completely eliminated, thus the basic layer achievable rate for structure-based decoding is* $R_{b,sb} = B\log_2(1+\frac{P_1}{\sigma^2})$. ■

Following the same argument, one can conclude that the "more structured"[†] the distribution of the secondary layer signal bears, the larger achievable rate of the basic layer will

[†]We loosely use the word "more structured" for lower order QAMs. The distribution of lower order QAM symbols is relatively less random than high order QAM symbols, e.g., QPSK vs. 16QAM.

be. In this sense, the Gaussian like secondary layer signal is the worst ILI case for basic layer demodulation.

3.4.1 Basic layer achievable rate derivation

In this section, we analyze the basic layer achievable rate assuming the second layer structure information is incorporated in decoding.

Lemma 2 *With the structure information from the secondary layer, the basic layer achievable rate is upper bounded by* $R_{b,sb} = B\log_2(1+\frac{P_1}{\sigma^2})$.

Proof. *As mentioned in Section II, the basic layer achievable rate with traditional demodulation/decoding (e.g., without exploiting the second layer structure information) is* $R_b = B\log_2(1+\frac{P_1}{P_2+\sigma^2})$. *Under the most extreme case where the secondary layer interference is deterministic, the ILI can be completely eliminated, thus the basic layer achievable rate for structure-based decoding is* $R_{b,sb} = B\log_2(1+\frac{P_1}{\sigma^2})$. ■

Following the same argument, one can conclude that the "more structured"[‡] the distribution of the secondary layer signal bears, the larger achievable rate of the basic layer will be. In this sense, the Gaussian like secondary layer signal is the worst ILI case for basic layer demodulation.

3.4.2 Basic layer achievable rate derivation

In order to arrive at the achievable rate, we must calculate the mutual information in consideration of the QAM-structured secondary layer interference. Rewrite the received signal as

$$Y = \sqrt{P}_1 x_1 + \underbrace{\underbrace{\sqrt{P}_2 x_2}_{\text{QAM noise}} + \underbrace{n.}_{\text{Gaussian noise}}}_{\bar{n}\text{: overall noise and interference}} \tag{3.17}$$

Also define the SINR for the basic layer as

$$SINR = \frac{P_1}{P_2 + \sigma^2}.$$

[‡]We loosely use the word "more structured" for lower order QAMs. The distribution of lower order QAM symbols is relatively less random than high order QAM symbols, e.g., QPSK vs. 16QAM.

In Equation (3.17), the transmitted QAM signal x_i $(i = 1, 2)$ and Gaussian noise n are complex numbers $x_i \in C$, $n \in C$. To simplify the derivation, we may think of each signal as a real 2-tuple in R^2, and only consider its real part due to symmetry.

Consider a standard $(M \times M)$-QAM signal set, which is the Cartesian product of two M-PAM sets; i.e.,

$$A = \{(a + ib)|a \in A', b \in A'\} \tag{3.18}$$

where $A' = \{-d(M-1)/2, ..., -d/2, d/2, ..., d(M-1)/2\}$. Take QPSK signal for example, $x_2 = \{\pm\frac{1}{\sqrt{2}}, \pm\frac{j}{\sqrt{2}}\}$, where $M = 2$, $A' = \{-\frac{\sqrt{2}}{2}, \frac{\sqrt{2}}{2}\}$. Similarly in 16QAM, $x_2 = \{\pm\frac{a}{\sqrt{10}}, \pm\frac{b}{\sqrt{2}}j\}$, where $a \in \{1, 3\}$, $b \in \{1, 3\}$. $M = 4$, $A' = \{-\frac{3}{\sqrt{10}}, -\frac{1}{\sqrt{10}}, \frac{1}{\sqrt{10}}, \frac{3}{\sqrt{10}}\}$. In general, the PDF of M-PAM signal is given by

$$f_{PAM}(x) = \frac{1}{M}\left(\sum_{\substack{k=1 \\ x_{i,k} \in A_i'}}^{M} \delta(x - \sqrt{P_2}x_{i,k})\right) \tag{3.19}$$

where $\delta(\cdot)$ denotes the Dirac delta function. $A_i^{'}$ $(i = 1, 2)$ denotes the M-PAM sets for basic and secondary layer, respectively. Here, we use $x_{i,k}$ to denote the kth symbol representative in M-PAM sets for basic and secondary layer, respectively.

With σ^2, the PDF of the i.i.d Gaussian noise can be written as

$$f_n(x) = \frac{1}{\sqrt{2\pi\sigma^2}} \cdot \exp(-\frac{x^2}{2\sigma^2}). \tag{3.20}$$

Since the effective overall noise (secondary interference plus Gaussian) for basic layer signal is given by

$$\overline{n} = \sqrt{P_2}x_2 + n, \tag{3.21}$$

its PDF can be calculated from the convolution $f_{\overline{n}}(x) = f_n(x) * f_{PAM}(x)$. Taking advantage

of the sifting property of Dirac delta function,

$$\begin{aligned} f_{\overline{n}}(x) &= f_n(x) * f_{PAM}(x) \\ &= \frac{1}{\sqrt{2\pi\sigma^2}} \cdot \exp(-\frac{x^2}{2\sigma^2}) * \frac{1}{M_2} \left(\sum_{\substack{k=1 \\ x_{2,k} \in A_2'}}^{M_2} \delta(x - \sqrt{P}_2 x_{2,k}) \right) \\ &= \frac{1}{M_2\sqrt{2\pi\sigma^2}} \left(\sum_{\substack{k=1 \\ x_{2,k} \in A_2'}}^{M_2} \exp(-\frac{(x - \sqrt{P}_2 x_{2,k})^2}{2\sigma^2}) \right). \end{aligned} \tag{3.22}$$

With the observation $y = \sqrt{P}_1 x_1 + \overline{n}$ and the effective overall noise distribution $f_{\overline{n}}(x)$ in hand, we can now compute the basic layer achievable rate

$$R_{b,sb} = I(x_1; y). \tag{3.23}$$

Since $\overline{n}$ is independent of the basic layer symbol x_1, $h(y|x_1) = h(\overline{n})$. Therefore

$$\begin{aligned} I(x_1; y) &= h(y) - h(y|x_1) \\ &= h(y) - h(\overline{n}). \end{aligned} \tag{3.24}$$

Firstly, we calculate $h(\overline{n})$ from

$$\begin{aligned} \log_2 f_{\overline{n}}(x) &= \log_2 \frac{1}{M_2\sqrt{2\pi\sigma^2}} \left(\sum_{\substack{k=1 \\ x_{2,k} \in A_2'}}^{M_2} \exp(-\frac{(x - \sqrt{P}_2 x_{2,k})^2}{2\sigma^2}) \right) \\ &= -\log_2 M_2 - \frac{1}{2}\log_2(2\pi\sigma^2) + \log_2 \left(\sum_{\substack{k=1 \\ x_{2,k} \in A_2'}}^{M_2} \exp(-\frac{(x - \sqrt{P}_2 x_{2,k})^2}{2\sigma^2}) \right) \end{aligned} \tag{3.25}$$

$$
\begin{aligned}
h(\overline{n}) &= -E[\log_2 f_{\overline{n}}(x)] \\
&= E\left[\log_2 M_2 + \frac{1}{2}\log_2(2\pi\sigma^2) - \log_2\left(\sum_{\substack{k=1 \\ x_{2,k}\in A_2'}}^{M_2} \exp(-\frac{(x-\sqrt{P}_2 x_{2,k})^2}{2\sigma^2})\right)\right] \\
&= \log_2 M_2 + \frac{1}{2}\log_2(2\pi\sigma^2) - E\left[\log_2\left(\sum_{\substack{k=1 \\ x_{2,k}\in A_2'}}^{M_2} \exp(-\frac{(x-\sqrt{P}_2 x_{2,k})^2}{2\sigma^2})\right)\right] \qquad (3.26) \\
&= \log_2 M_2 + \frac{1}{2}\log_2(2\pi\sigma^2) - \int \log_2\left(\sum_{\substack{k=1 \\ x_{2,k}\in A_2'}}^{M_2} \exp(-\frac{(x-\sqrt{P}_2 x_{2,k})^2}{2\sigma^2})\right)\cdot f_{\overline{n}}(x)dx.
\end{aligned}
$$

Then we calculate $h(y)$ by computing

$$
p(y) = \sum_{\substack{k=1 \\ x_{1,k}\in A_1'}}^{M_1} p(y|x_{1,k})p(x_{1,k}) \qquad (3.27)
$$

where A_1' denotes the M-PAM sets for the basic information layer. $x_{1,k}$ denotes the kth symbol representative in the A_1'. Since $x_{1,k}$ is uniformly distributed in the sets A_1', $p(x_{1,k}) = 1/M$.

$$
\begin{aligned}
p(y) &= \sum_{\substack{k=1 \\ x_{1,k}\in A_1'}}^{M_1} p(y|x_{1,k})p(x_{1,k}) = \frac{1}{M_1}\sum_{\substack{k=1 \\ x_{1,k}\in A_1'}}^{M_1} p(y|x_{1,k}) = \frac{1}{M_1}\sum_{\substack{k=1 \\ x_{1,k}\in A_1'}}^{M_1} f_{\overline{n}}(y-\sqrt{P}_1 x_{1,k}) \\
&= \frac{1}{M_1 M_2\sqrt{2\pi\sigma^2}}\sum_{\substack{k=1 \\ x_{1,k}\in A_1'}}^{M_1}\sum_{\substack{k'=1 \\ x_{2,k'}\in A_2'}}^{M_2} \exp(-\frac{(y-\sqrt{P}_1 x_{1,k}-\sqrt{P}_2 x_{2,k'})^2}{2\sigma^2}). \qquad (3.28)
\end{aligned}
$$

We now arrive at

$$
h(y) = -\int \log_2(p(y))p(y)dy, \qquad (3.29)
$$

which can be numerically integrated by plugging in Equation (3.28). Finally, by combining Equation (3.29) and Equation (3.26) into Equation (3.24), we arrive at the horizontal M-PAM achievable rate expression. The same methodology can be applied for computing the vertical M-PAM achievable rate.

Fig. 3.6 and Fig. 3.7 show the basic layer achievable rate curves, $R_{b,sb}$, for QPSK+QPSK and QPSK+16QAM HM schemes with different power ratio λ, respectively. It is worth noting that, when $\lambda = \infty$ the secondary layer interference is purely Gaussian noise, which is the worst case for HM system (the lower bound of all achievable rate curves) as explained in *Lemma* 1. As can be observed in Fig. 3.6 and Fig. 3.7, when λ is small (e.g., 6 dB, indicating the secondary layer signal power P_2 is relatively large), the structure-based decoding approach demonstrates noticeable SINR gain when compared to achievable rate curve with $\lambda = \infty$. Depending on the data rate, 0-6 dB SINR gain for the QPSK+QPSK case and 0-5.7 dB SINR gain for the QPSK+16QAM case can be achieved. In addition, the SINR gain becomes larger when achievable rate is higher. This fact validates the importance of the structure-based decoding approach. When λ is large (beyond 10 dB), meaning the secondary layer signal power P_2 is relatively small (e.g., when the Gaussian noise n dominates the overall noise $\overline{\mathbf{n}}$), the structure-based decoding achievable rate curves $R_{b,sb}$ are only marginally higher than the achievable rate curve with $\lambda = \infty$, especially at lower rate. The SINR gain diminishes when λ reaches 15 dB for QPSK+QPSK case.

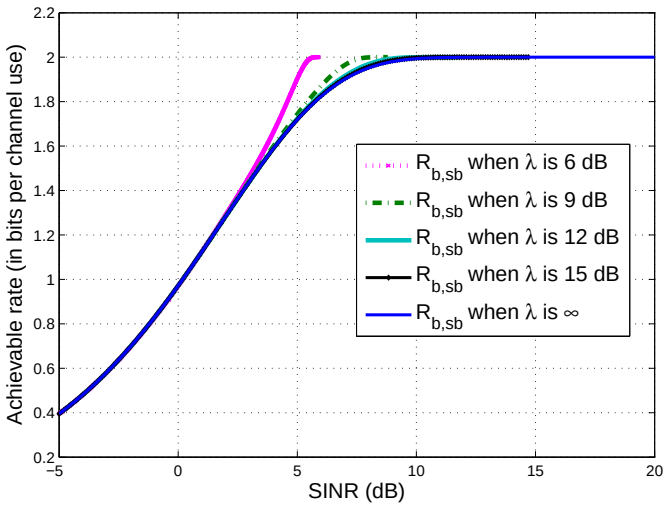

Figure 3.6: The basic layer achievable rate for QPSK+QPSK HM with different power ratio under AWGN channel.

It is interesting to note that, the basic layer achievable rate $R_{b,sb}$ is different for QPSK+QPSK

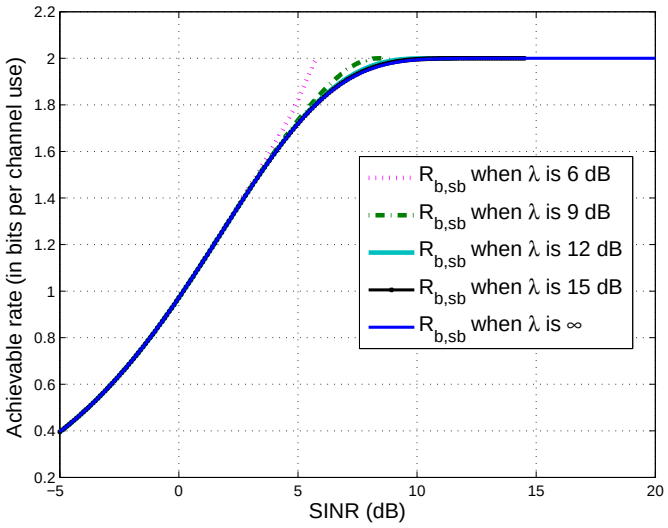

Figure 3.7: The basic layer achievable rate for QPSK+16QAM HM with different power ratio under AWGN channel.

and QPSK+16QAM schemes at same λ. Fig. 3.8 illustrates the achievable rate curves for these two schemes at low power ratio (6 dB). At the same λ, the basic layer achievable rate for QPSK+QPSK scheme is larger than that for QPSK+16QAM, especially at high rate, which implies the secondary layer structures have a direct impact on the basic layer achievable rate. Intuitively, the 16QAM constellation is less "structured" compared to the QPSK constellation, hence is a "worse" interference to the basic layer. We can conjecture that as the secondary layer constellation order increases, $R_{b,sb}$ will eventually approach the achievable rate curve with $\lambda = \infty$.

3.5 Performance analysis and Numerical results

In this section, we evaluate the basic layer BER performance for LDPC coded QPSK+QPSK HM signal using the structure-based decoding approach and other decoding approaches. The simulation settings are the same as mentioned in Section III (c): each layer of the HM constellation is independently Gray mapped, the number of LDPC decoder inner iterations is 40 for all the decoding approaches, the LDPC codes is specified in [33] with code length 9216

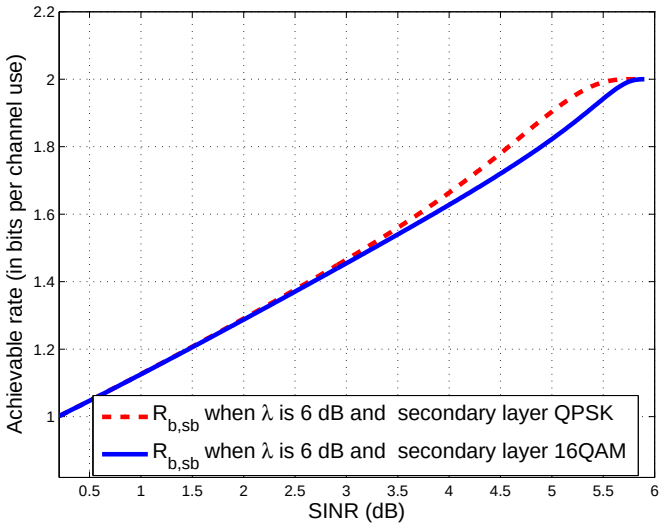

Figure 3.8: The achievable rate comparison for the basic layer between QPSK+QPSK and QPSK+16QAM HM schemes with the same power ratio.

and code rate 3/4, the number of outside iterations for the multi-layer iterative decoding approach is 5.

Fig. 3.9 shows the basic layer BER curves for the QPSK+QPSK HM signal (λ is 6 dB) when adopting with the traditional decoding (e.g., without taking account of the secondary layer structure information), the structure-based decoding and the multi-layer iterative decoding respectively. The SINR bound corresponding to the achievable rate $R_{b,sb} = 3/2$ (due to the LDPC code rate is 3/4), is provided as a reference. It is seen that the performance of basic layer when using the structure-based decoding is 0.3 dB better than the traditional decoding, which is a noticeable improvement under AWGN channel. The structure-based decoding achieves almost the same BER performance as the much more complicated multi-layer iterative decoding for the basic layer reception. The results indicate that the structure-based decoding approach achieves an excellent performance-complexity trade-off in the HM scenario, specially for small λ (e.g. λ between 6 dB and 9 dB). Compared with the theoretical limit, it can be seen that the structure-based decoding BER curve has a 0.6 dB gap from the theoretical SINR for $R_{b,sb} = 3/2$, which can primarily attributed to the sub-optimality

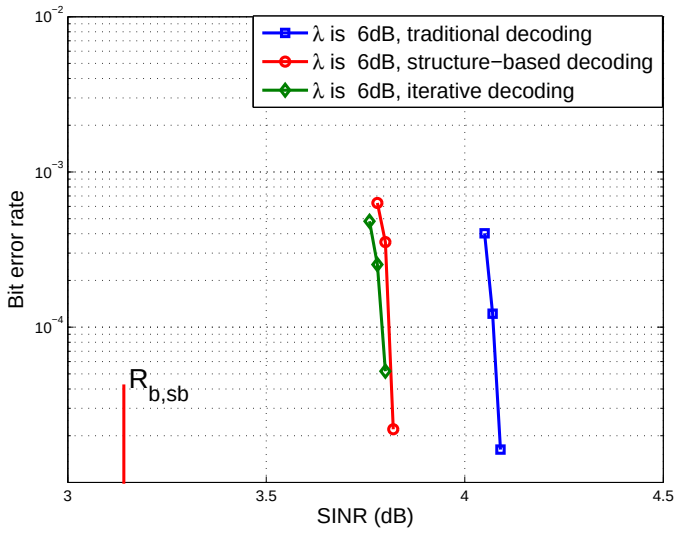

Figure 3.9: BER versus SINR using 3/4 rate LDPC for the basic layer of QPSK+QPSK HM, power ratio λ is 6 dB.

of the LDPC codes.

When λ is raised to 15 dB, as shown in Fig. 3.10, the BER curves of the three decoding approaches almost merge, in this case the advantage of the structure-based decoding approach becomes negligible. This is not surprising since the AWGN noise becomes a dominating factor in $\overline{n}$ when λ becomes larger. The basic layer BER curve of the structure-based decoding in this example will be eventually overlap with the BER curve of QPSK under AWGN channel as λ goes to infinity. This phenomenon perfectly matches the achievable rate curves in Fig. 3.6.

3.6 Algorithm Implementation

The structure-based LDPC decoding algorithm is applied to real world signals collected from our newly designed Broadband Digital Radio (BDR) system. As part of its key features, HM allows the BDR to offer layered services in both FM and AM bands. The block diagram of the HM mode in BDR is shown in the Fig. 3.11, the feature blocks include an LDPC encoder, a HM mapper and an OFDM modulator. Here we only focus on the basic layer

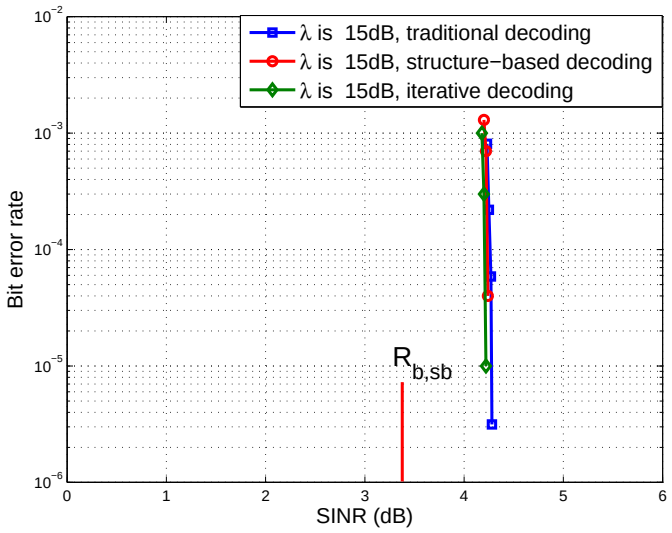

Figure 3.10: BER versus SINR using 3/4 rate LDPC for the basic layer of QPSK+QPSK HM, power ratio λ is 15 dB.

detection, the secondary layer information bits can be decoded by using successive decoding strategy.

3.7 Conclusions

This chapter presented a structure-based decoding algorithm for hierarchical QAM modulation. By exploiting the structure information of the secondary layer, the proposed decoding algorithm effectively mitigates the ILI for the basic layer in HM reception. Performance and complexity comparisons with the multi-layer iterative decoding approach are presented. These comparisons reveal that the proposed decoding algorithm achieves an excellent performance-complexity tradeoff over the existing decoding approaches. In addition, the basic layer achievable rate has been derived to quantify the theoretical improvement due to structure-based decoding - the SINR gain is as significant as 6 dB at 2 bit/Hz in the QPSK+QPSK HM transmission. Numerical results from simulations and a real-world digital radio broadcasting system are provided to illustrate the efficacy of the proposed technique.

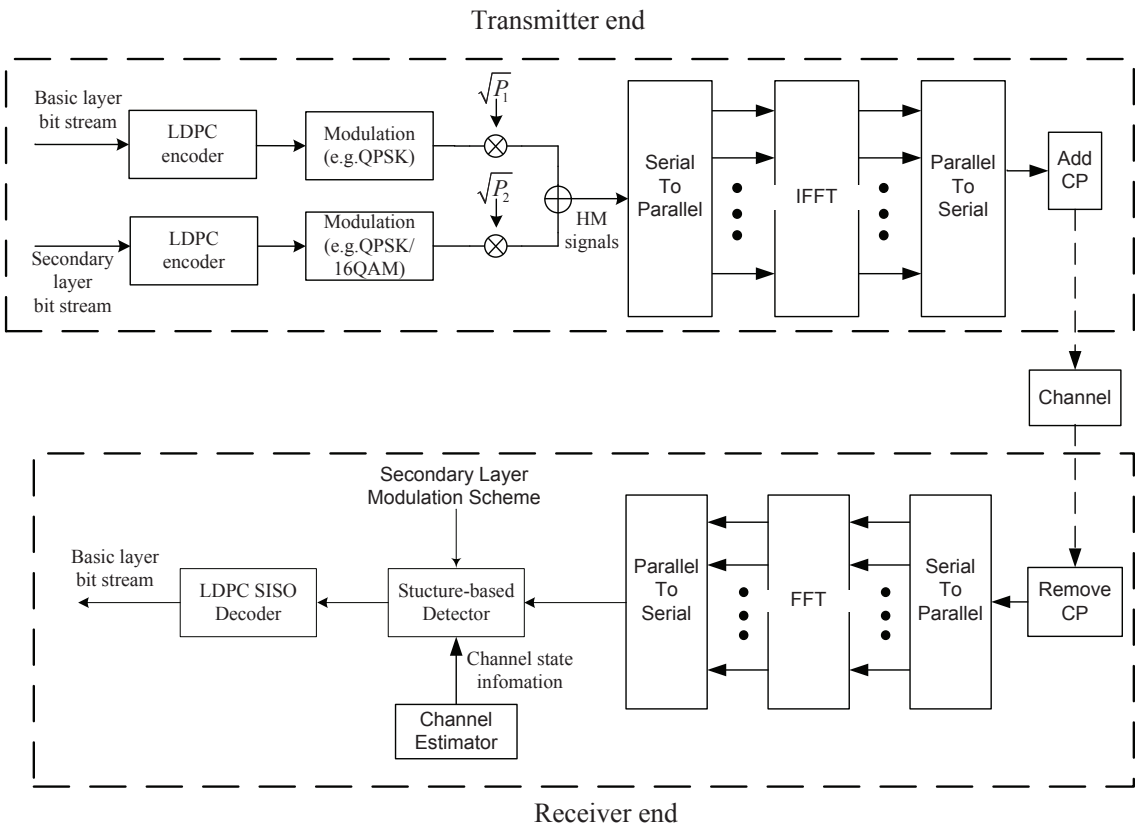

Figure 3.11: Block diagram of HM mode in BDR.

Chapter 4

A LOW-COMPLEXITY DECODING ALGORITHM FOR CODED HIERARCHICAL MODULATION IN SINGLE FREQUENCY NETWORKS

For the digital network, frequency planning is needed as in other digital broadcasting signals. Most importantly, the single frequency network (SFN) architecture will be used in the Broadband Digital Radio (BDR) deployment. In the BDR networks, the hierarchical modulation (HM) technique is adopted to provide both global and local information. Except the inter-layer interference (ILI) which is explained in Chapter 3, the HM based SFN also introduces the inter-cell interference (ICI). In this chapter, we develop a low-complexity successive interference cancellation (SIC) algorithm for the coded HM signals, which can effectively mitigate both the ILI and ICI in the SFN.

4.1 Hierarchical Modulation in Single Frequency Networks

How to increase the spectral efficiency of digital broadcasting systems has been a topic of extensive studies in the past years. Among other techniques proposed, the single frequency network (SFN) [36], [37] is one of the most important schemes for efficient utilization of the radio spectrum in digital broadcasting. Different from the multi-frequency network (MFN) where each station makes use of a different transmitting frequency, in an SFN all the transmitters broadcast the same signal on the same frequency within the whole coverage area. Besides the spectrum efficiency, the SFN increases the coverage area and decreases the transmission power/outage probability [38] by virtue of overlapping coherent signals from the transmitters. The benefit of the SFN can be quantified as the "SFN gain", which is investigated in [39], [40]. On the other hand, due to the transmission of identical global information from different transmitters, local services are no longer possible in a typical SFN.

In order to accommodate the local services, e.g., local news, traffic information, weather

reports or local alerts, two classes of technologies have been investigated for the SFN: the first one is the time slicing approach [41], whereas the second one is the hierarchical modulation approach [43]-[47]. Both approaches can be applied in conjunction with the SFN to provide both global and local information.

Time slicing technique (which is included in DVB-H) consists of temporal multiplexing of services to be transmitted. The main idea behind it is to establish two types of time slices: one used for transmitting the global content and the other for delivering the local content. Besides providing the local service, the time slicing technique is still capable of transmitting the global service with all SFN advantages. However, in order to separate the global contents and local contents, the adaptation intervals are needed to ensure that no data from the global services is mixed with the data from the local services. The overhead generated by adaptation intervals reduces the efficiency of the entire networks and results in the discontinuous transmission. The advantages and limitations of time slicing are investigated in [41].

The second approach for delivering the local services in an SFN is the usage of hierarchical modulation (HM), which is already in the DVB-T/H/SH standards [15]-[42]. Compared with the time slicing technique, the HM provides continuous transmission without adding the overhead. It enables the transmission of global services over the SFN, and at the same time, local contents within the vicinity of the transmitter on the same frequency band. Different from the traditional single-layer SFN, each transmitter in the HM-based SFN provides multiple layers of data streams. Each layer has a different carrier to noise ratio (C/N) threshold and a corresponding coverage area, all within the same transmission bandwidth. In this chapter, we use the term the *basic layer* signal to describe the global services data transmitted in the HM-based SFN; the local services data that is added on top of the basic layer will be named the *secondary layer* signal.

The flexibility of HM-based SFN does not come without a cost. Two primary interferences lead to the loss of the achievable symbol rate in the HM-based SFN. The first type of interference is called the inter-layer interference (ILI) [32], the added secondary layer of each transmitter not only reduces the effective transmission power from the basic layer, but also incurs an additional inference to the basic layer reception; The second type of interference

is called the inter-cell interference (ICI), the basic layer and secondary layer signals from different transmitters may become interferences for each other in the overlapping area.

Most HM systems adopt the powerful channel codes (e.g., Turbo codes, low-density parity-check code (LDPC)) for better fading resistance and higher receiver sensitivity [24]-[28]. In order to cope with the ILI and ICI, the decoding algorithm for the coded signals in the HM-based SFN should be carefully investigated. To date, there is limited research work focusing on the decoding algorithm in the HM-based SFN scenario. As mentioned in [43], the multi-layer iterative decoding approach [32], [30], [31] might be applied to the HM-based SFN scenario. This type of approach can effectively mitigate the ILI and ICI, since all the layers (the shared basic layer and different secondary layers in the SFN) keep refining the reception quality during the iterations, even though the detectable layers might be part of them*. However, the primary limitations of the multi-layer iterative decoding approach are its high decoding complexity/delay and the large memory requirement, especially in the HM-based SFN scenario where part of the decoder resources is used on the unwanted layers. In addition, the number of outside iterations (iterations between the demodulator and channel decoder) and inner iterations (iterations inside the channel decoder) must be tuned in order to achieve the best performance. This could be problematic with changing signal-to-noise-plus-interference ratio (SINR) values and channel characteristics. Therefore a more efficient decoding algorithm with low-complexity is highly desirable for the coded HM signal in the SFN.

The main contributions of this chapter are two-fold. First, we investigate the decoding algorithms in the HM-based SFN, which can effectively mitigate the ILI and ICI problems. To date, this topic has not been studied in detail in the literature. In particular, we propose a low-complexity structured successive interference cancellation (SIC) approach for coded HM signal in the SFN, which can practically address the performance loss caused by the QAM-structured (quadrature amplitude modulation) ILI and ICI directly at the receiver end. Compared with the traditional SIC method [29], the main difference of the structured SIC approach is that we consider the mapping information (e.g., QPSK, 16QAM) of the

*In the HM SFN, the weak secondary signals which are far from the mobile users cannot be detected due to the path loss or fading.

secondary layer signals when decoding the coded bits. Also the decoding complexity of the proposed approach is much lower than that of the multi-layer iterative decoding method [30], [31] without much performance loss. Secondly, we evaluate the performance of structured SIC approach in a real-world OFDM-based broadband digital radio (BRD) system [34]. The simulations show that the structured SIC approach can offer 0-0.7 dB carrier to noise ratio C/N gain compared with the traditional SIC approach, while providing the comparable performance with the multi-layer iterative decoding approach. The performance evaluation and decoding complexity comparisons indicate that the proposed structured SIC approach offers a good performance-complexity trade-off. Besides the low decoding complexity, another big advantage of the structured SIC approach is its compatibility. It can be applied to different soft-decision channel coding schemes (e.g., LPDC, Turbo code) and mappings schemes under various channel profiles.

The rest of the chapter is organized as follows. Section 4.2 describes the coded HM-based SFN system, which can provide both global and local information on the same frequency band. Section 4.3 puts forth the structured SIC approach for the coded HM signals in the SFN and analyzes its advantages. The decoding complexity analysis and comparisons are provided in Section 4.4. Section 4.5 first introduces the algorithm implementation in the BDR SFN networks, and then evaluates the bit error rate (BER) performance of the structured SIC approach against the traditional SIC approach and the multi-layer iterative decoding approach. Finally, a conclusion is drawn in Section 4.6.

4.2 The Proposed Coded HM-based SFN

In this section, we first illustrate a practical HM-based SFN example, and then the system model and definitions are provided.

4.2.1 HM-based SFN

Fig. 4.1 illustrates a practical example which involves two transmitters (TX) broadcasting their own QPSK+QPSK HM signals† over the SFN. These two transmitters share the same

†QPSK+QPSK HM signal indicates the basic layer and the secondary layer are both QPSK mapped. The two layer QPSK signals constitute a non-uniform 16QAM.

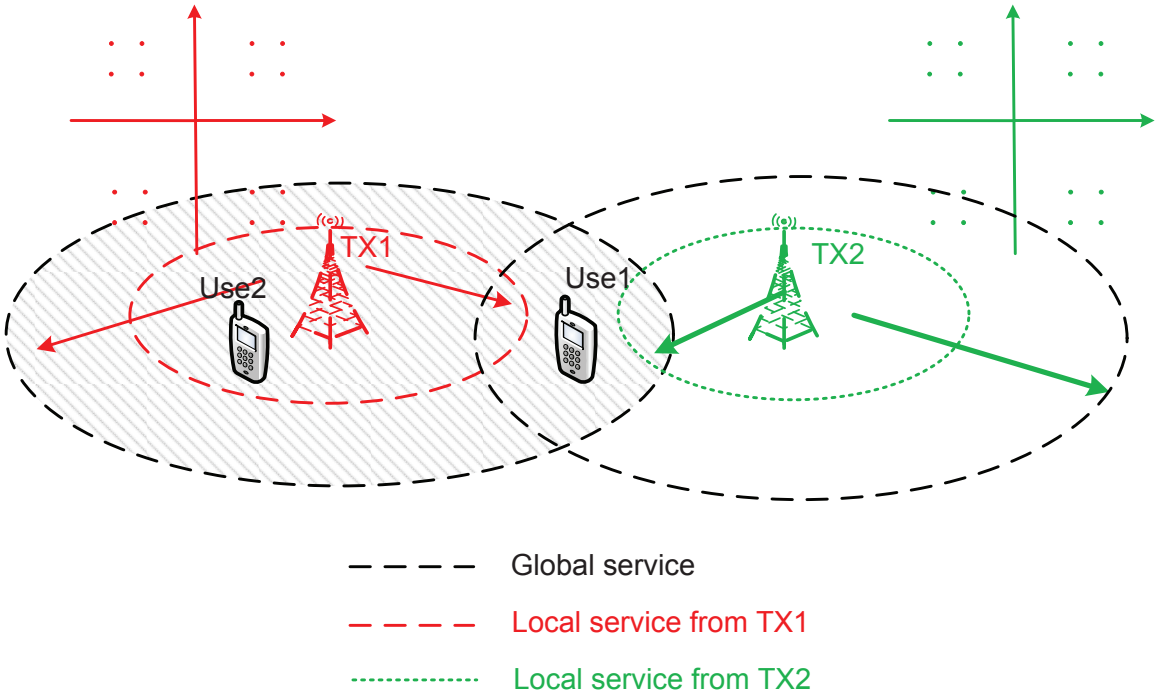

Figure 4.1: Two transmitters broadcast their own QPSK+QPSK HM signals over the SFN.

basic layer QPSK signal, which conveys the global service data within the SFN coverage. The secondary layer QPSK signal of each transmitter is unique, carrying the local service data in its own coverage, which is determined by the secondary layer transmission power. In the HM-based SFN, the received signal contains different components with various strengths. In this example, the received signal has one strong basic layer component (global service data) and two relatively weak secondary layer components (local service data from each transmitter). Depending on the location and the size/complexity constraints of the mobile users, the detectable signal can be the global service data (e.g., User1 in the figure, which is out of the local coverage), or the global service data together with the local service data (e.g., User2 in the figure, which is within the local coverage of TX1).

4.2.2 System Model and Definitions

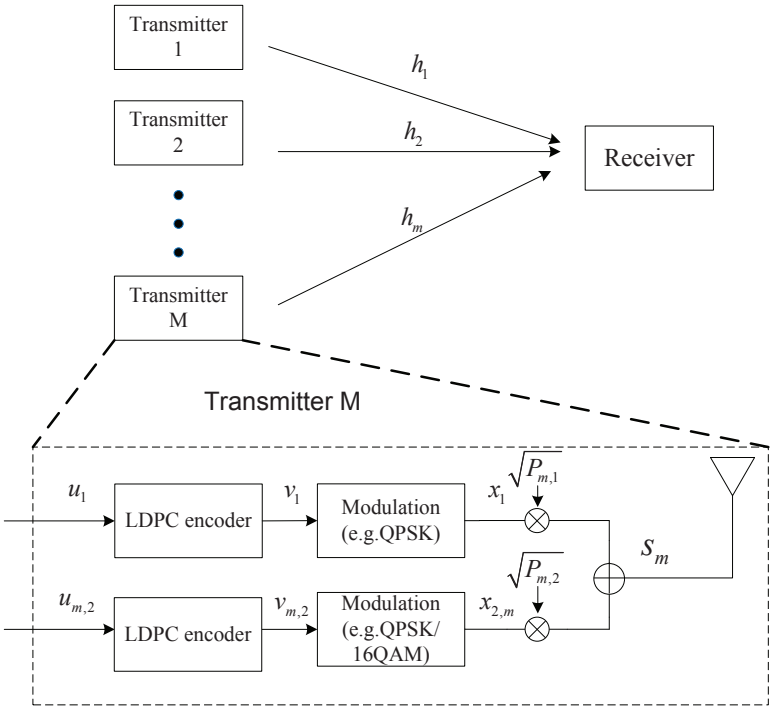

Figure 4.2: M transmitters simultaneously send coded HM signals to a receiver over the SFN.

In theory, multi-layer source information of each transmitter can be delivered to users experiencing different channel qualities through HM. In this chapter, only the two-layer HM transmission is investigated, which is sufficient for practical wireless systems (e.g., a QPSK+16QAM HM signal can provide the non-uniform 64QAM constellation). We denote symbol alphabet $\mathbf{u}_1$ as the shared basic layer information bits (global service) for all the transmitters, and $\mathbf{u}_{m,2}$ as the unique secondary layer information bits (local service) for the mth transmitter. $\mathbf{v}_1$ and $\mathbf{v}_{m,2}$ denotes the corresponding coded bits after channel encoder (in this chapter, we assume LDPC as the coding choice): $\mathbf{v}_1 = [v_1^1, ..., v_1^n]^T$ and $\mathbf{v}_{m,2} = [v_{m,2}^1, ..., v_{m,2}^n]^T$, where v_1^n and $v_{m,2}^n$ is the nth coded bit of basic layer and secondary layer, respectively. The two-layer coded bits are then modulated into $\mathbf{x}_1$ and $\mathbf{x}_{m,2}$, $\mathbf{x}_1 = [x_1^1, ..., x_1^k]^T$ and $\mathbf{x}_{m,2} = [x_{m,2}^1, ..., x_{m,2}^k]^T$, where x_1^k and $x_{m,2}^k$ denotes the kth symbol of basic layer and secondary layer respectively.

Fig. 4.2 illustrates the transmission in the HM-based SFN with M transmitters [‡] simultaneously sending coded HM signals to a receiver over the SFN. The two data streams $\mathbf{u}_1$ and $\mathbf{u}_{m,2}$ of the mth transmitter are independently coded using the LDPC encoders and then modulated using QAM with amplitude set to be $\sqrt{P_{m,1}}$ and $\sqrt{P_{m,2}}$, respectively. Finally, the symbols from the two layers are superimposed into $\mathbf{s}_m$ before transmission. Mathematically, the transmitted signal is given by

$$\mathbf{s}_m = \sqrt{P_{m,1}}\mathbf{x}_1 + \sqrt{P_{m,2}}\mathbf{x}_{m,2}, \tag{4.1}$$

with $P_{m,1} + P_{m,2} = P_m$, where P_m is total transmission power of the mth transmitter, $\mathbf{s}_m = [s_m^1, ..., s_m^k]^T$. More precisely, the secondary layer symbols $\mathbf{x}_{m,2}$ in Equation (4.1) should be written as $\mathbf{x}_{m,2}(\mathbf{x}_1)$ to emphasize its dependency on $\mathbf{x}_1$ (e.g., the Gray mapping [15][14]). Since the notation $\mathbf{x}_{m,2}$ does not affect our derivation of the proposed decoding approach, we use $\mathbf{x}_{m,2}$ here for convenience.

Also we define the power ratio between the basic layer signal and the secondary layer for the mth transmitter,

$$\lambda_m = \frac{P_{m,1}}{P_{m,2}}, \tag{4.2}$$

In the HM-based SFN, λ_m is an important parameter that determines the power allocation for the global service data and local service data. In the extreme case when $\lambda_m = \infty$, all the transmission power is assigned to the basic layer, thus the transmitter only broadcasts the global service data. Also the λ_m characterizes the constellation of hierarchical signals, for example when $\lambda_m = 6$ dB, the QPSM+QPSK HM constellation becomes the uniform 16QAM.

At the receiver side, a user with low signal strength simply demodulates/decodes the shared basic layer information, whereas users with higher signal strength can demodulate/decode not only the basic layer information, but also the specific secondary layer information from the nearby transmitters. At the receiver end, the kth received symbol can

[‡] M is usually less than 4 in the real scenario, when some transmitters in the SFN are far from the mobile user, the interference from them can be neglected due to the path loss.

be expressed as

$$\begin{aligned} y_k &= \sum_{m=1}^{M} h_m^k s_m^k + n_k. \\ &= \sum_{m=1}^{M} h_m^k (\sqrt{P_{m,1}} x_1^k + \sqrt{P_{m,2}} x_{m,2}^k) + n_k \\ &= (\sum_{m=1}^{M} h_m^k \sqrt{P_{m,1}}) x_1^k + \sum_{m=1}^{M} h_m^k \sqrt{P_{m,2}} x_{m,2}^k + n_k. \end{aligned} \tag{4.3}$$

where y_k is the kth received symbol; s_m^k is the kth transmitted symbol from the mth transmitter and h_m^k is corresponding frequency domain channel response; n_k is the Gaussian noise added on the kth received symbol. It can be observed that the basic layer signal strength can be reduced due to different channel phases. In these cases, the secondary layer ICI on the basic layer is particularly large.

4.3 Structured SIC approach for HM-based SFN

As mentioned in Section 4.1, demodulation/decoding of coded HM signals in the SFN suffers from ILI and ICI. Although the multi-layer iterative decoding approaches can provide good interference mitigation in the HM-based SFN, the costs paid are the high decoding complexity/delay and memory requirements. In this section, we first present a structured demodulation/decoding algorithm that takes advantage of the QAM structure of secondary layer signals as the side information. The new decoding algorithm can largely cancel out the ILI and ICI without causing too much complexity increase. Subsequently, we analyze the advantages of the proposed decoding algorithm. Finally, the decoding complexity analysis and comparison for different decoding approaches are provided.

The structure SIC approach is motivated by the following observation. In QAM-based HM broadcasting over the SFN, the modulation schemes of each transmitter (both basic and secondary layers) is sent over a control channel. As a result, the QAM mapping information (e.g., QPSK, 16QAM) of the secondary layer is available for the demodulation/decoding. In other words, the mapping from the $l_{m,2}$ information bits onto the kth secondary layer symbol $x_{m,2}^k$ of the mth transmitter is known as the prior information: $(v_{m,2}^1, ..., v_{m,2}^{l_{m,2}})^k \rightarrow x_{m,2}^k$, where $(v_{m,2}^1, ..., v_{m,2}^{l_{m,2}})^k$ is the kth random vector that spans $\{0,1\}^{l_{m,2}}$. Based on the extra

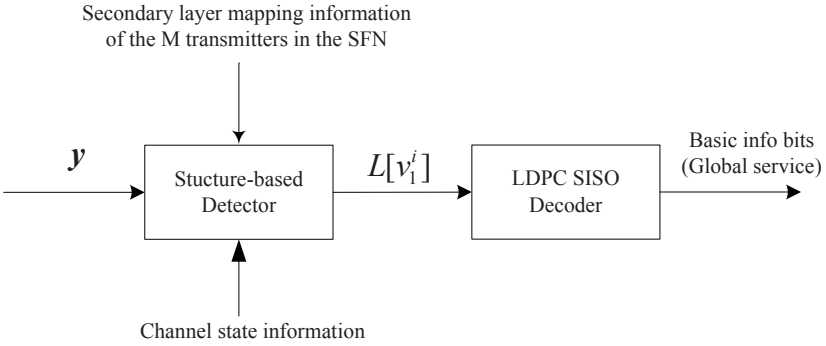

Figure 4.3: Structured demodulation/decoding for the basic layer (global service data).

mapping information, Equation (4.3) can be rewritten as

$$\begin{aligned} y_k &= (\sum_{m=1}^{M} h_m^k \sqrt{P_{m,1}}) x_1^k(v_1^1, ..., v_1^{l_{m,1}}) + \sum_{m=1}^{M} h_m^k \sqrt{P_{m,2}} x_{m,2}^k(v_2^1, ..., v_2^{l_{m,2}}) + n_k \\ &= h_{all}^{'} x_1^k(v_1^1, ..., v_1^{l_{m,1}}) + \sum_{m=1}^{M} h_m^{'} x_{m,2}^k(v_2^1, ..., v_2^{l_{m,2}}) + n_k, \end{aligned} \tag{4.4}$$

where $l_{m,1}$ and $l_{m,2}$ denote the number of the information bits mapped into a basic layer symbol (since the basic layer symbol is same in the HM SFN, $l_{m,1} \equiv l_1$) and a secondary symbol, respectively; $h_{all}^{'} = (\sum_{m=1}^{M} h_m^k \sqrt{P_{m,1}})$; $h_m^{'} = h_m^k \sqrt{P_{m,2}}$.

Instead of being simply treated as the Gaussian noise [43], the distribution of the secondary layer signals in the SFN can be further exploited to refine the metric for the Log-likelihood ratio (LLR) calculation. With the above observation we are ready to demonstrate the proposed structured SIC approach, which contains two stages: (1) the basic layer (global service data) decoding; (2) the secondary layer (local service data) decoding if necessary, depending on the signal strength of the secondary layer.

4.3.1 Basic Layer Decoding

The structured SIC approach first extracts the global content from the received signal. Unlike the traditional basic layer QAM demodulators[§], the structure-based detector produces

[§]The traditional QAM demodulators calculate the Log-likelihood ratio (LLR) only based on the observation y_k, and treat the undetected symbols and noise together as Gaussian noise.

the refined Log-likelihood ratio (LLR) by accounting for the mapping information of the secondary layer signals and the channel state information (CSI), as illustrated in Fig. 4.3. The modified LLR expression for the basic layer coded bits is shown in Equation (4.5). To simply the expression, we use the notation $x_{m,2}^k \triangleq x_{m,2}^k(v_{m,2}^1, ..., v_{m,2}^{l_{m,2}})$, which denotes different binary bit sequences $(v_{m,2}^1, ..., v_{m,2}^{l_{m,2}})$ are mapped to their corresponding constellation points $x_{m,2}^k$.

$$
\begin{aligned}
L(v_1^i) &= \log \frac{P[y_k|v_1^i = 0; (h_m^{'})_{m=1}^M; \text{mapping information of } \left(x_{m,2}^k\right)_{m=1}^M]}{P[y_k|v_1^i = 1; (h_m^{'})_{m=1}^M; \text{mapping information of } \left(x_{m,2}^k\right)_{m=1}^M]} \\
&= \log \frac{\sum\limits_{\left((v_{m,2}^1,...,v_{m,2}^{l_{m,2}}) \in \{0,1\}^{l_{m,2}}\right)_{m=1}^M} P[y_k|v_1^i = 0; (h_m^{'})_{m=1}^M; \left(x_{m,2}^k\right)_{m=1}^M] \cdot \prod\limits_{m=1}^M P(x_{m,2}^k)}{\sum\limits_{\left((v_{m,2}^1,...,v_{m,2}^{l_{m,2}}) \in \{0,1\}^{l_{m,2}}\right)_{m=1}^M} P[y_k|v_1^i = 1; (h_m^{'})_{m=1}^M; \left(x_{m,2}^k\right)_{m=1}^M] \cdot \prod\limits_{m=1}^M P(x_{m,2}^k)} \\
&= \log \frac{\sum\limits_{\left((v_{m,2}^1,...,v_{m,2}^{l_{m,2}}) \in \{0,1\}^{l_{m,2}}\right)_{m=1}^M} \exp\left\{-D\left[v_1^i = 0; (h_m^{'})_{m=1}^M; \left(x_{m,2}^k\right)_{m=1}^M\right]\right\}}{\sum\limits_{\left((v_{m,2}^1,...,v_{m,2}^{l_{m,2}}) \in \{0,1\}^{l_{m,2}}\right)_{m=1}^M} \exp\left\{-D\left[v_1^i = 1; (h_m^{'})_{m=1}^M; \left(x_{m,2}^k\right)_{m=1}^M\right]\right\}}, \quad (4.5)
\end{aligned}
$$

where the notation $(\cdot)_{m=1}^M$ denotes the variables for all the M secondary layers, and

$$
D\left[v_1^i = 0; (h_m^{'})_{m=1}^M; \left(x_{m,2}^k\right)_{m=1}^M\right] \doteq \frac{1}{2\sigma^2}||y_k - h_{all}^{'} x_1^k(v_1^1, ...v_1^{i-1}, 0, v_1^{i-1}, ...v_1^{l_1}) - \sum_{m=1}^M h_m^{'} x_{m,2}^k||^2 \quad (4.6)
$$

$$
D\left[v_1^i = 1; (h_m^{'})_{m=1}^M; \left(x_{m,2}^k\right)_{m=1}^M\right] \doteq \frac{1}{2\sigma^2}||y_k - h_{all}^{'} x_1^k(v_1^1, ...v_1^{i-1}, 1, v_1^{i-1}, ...v_1^{l_1}) - \sum_{m=1}^M h_m^{'} x_{m,2}^k||^2. \quad (4.7)
$$

Since the secondary layer symbols $x_{m,2}^k$ are independently and uniformly distributed on their own constellations, the term $\prod\limits_{m=1}^M P(x_{m,2}^k)$ can be cancelled out in Equation (4.5), which will reduce the number of multiplications in the LLR computation. With the modified LLR, we can pass them into the soft-input-soft-output (SISO) LDPC decoder and start decoding iteration (the decoding procedure is the same as we described in Chapter 3).

4.3.2 Secondary Layers Decoding

The main idea of the secondary layers decoding is to subtract the already-detected basic layer signals from the received signals firstly, and then decode the detectable secondary layers (when the average signal strength is larger than a the sensitivity of the receiver, the signal is detectable. The signal strength can be estimated through channel estimation. The details of channel estimation in the HM-based SFN and related pilots design can refer to [43], which is beyond the scope of this chapter). The procedures of secondary layer decoding are described as follows.

- *Initialization* **:**

step 1: For the secondary layer signals detection, firstly we need to demodulate the basic layer signal x_1^k and then subtract it from the received signal y_k.

$$\begin{aligned} y_k^{'} &= y_k - h_{all}^{'} x_1^k(v_1^1, ..., v_1^{l_1}) \\ &= \sum_{m=1}^{M} h_m^{'} x_{m,2}^k(v_{m,2}^1, ..., v_{m,2}^{l_{m,2}}) + n_k. \end{aligned}$$

step 2: Calculate the average signal strength from the mth secondary layer: $\overline{h_m^{'}} = E[h_m^{'}]$, where $E[\cdot]$ denotes the expectation operation. Then arrange the sequence $(\overline{h_1^{'}}, ..., \overline{h_m^{'}})$ in the descending order of the norm, let $h_{(j)}^{'}$ denote the jth largest elements of the sequence, than $y_k^{'}$ can be rewrite as:

$$y_k^{'} = \sum_{j=1}^{M} h_{(j)}^{'} x_{(j),2}^k + n_k.$$

After the two steps initialization, we are ready to start the structured SIC from the secondary layer signal with the largest $h_{(j)}^{'}$. Here we use the notation $x_{(j),2}^k \triangleq x_{(j),2}^k(v_{(j),2}^1, ..., v_{(j),2}^{l_{(j),2}})$ to simply the expression, also we set the counter C to record the index of SIC branches, $C = 0$ at the beginning.

- *Iteration* **:**

step 1 (structured decoding): The decoding principle is the same as the basic layer decoding, which explores the mapping information of the remaining secondary layer signals.

The refined LLR for the secondary layer is fed into the SISO LDPC decoder, and start the decoding iterations.

step 2 (updating):

$$\begin{aligned} y_k^{'} &= y_k^{'} - h_{(1)}^{'} x_{(1)}^k; \\ C &= C + 1; \\ h_{(1)}^{'} &= h_{(C+1)}^{'}. \end{aligned}$$

- *Stopping criteria* **:** When the average signal strength $h_{(1)}^{'}$ is less the sensitivity of the receiver or $C = M$, the secondary layers decoding are ended.

4.3.3 Advantages of the proposed algorithm

The proposed structured SIC approach has a number of advantages shown as follows, which are particularly important in the real system implementation.

- Low decoding complexity with good ILI/ICI mitigation: Different from the multi-layer iterative decoding approaches, which need to decode all the layers iteratively to provide good interference mitigation, the structured SIC approach only decodes the detectable signals without iterations, thus largely reducing the decoding complexity. In addition, under the HM-based SFN scenarios, the proposed approach provides comparable BER performance of the detectable signals with that of multi-layer iterative decoding approaches (see Section 4.5). All the comparisons indicate that the proposed structured SIC approach offers a good performance-complexity trade-off, particularly for the HM-based SFN scenarios.

- Suitable for different soft-decision channel coding and channel profiles: In the algorithm description above, we assume LDPC as the channel coding choice. Also the refined LLR calculation metric in the structure-based detector can be applied to other soft-decision channel codes (e.g., Turbo code) and various channel profiles. This significant compatibility allows other coded HM systems to adopt the proposed decoding algorithm.

- Simple constellation mapping rules: In [32], the optimized Gray mappings on the overall HM constellations (e.g., non-uniform 16QAM and non-uniform 64QAM) are proposed for good decoding performance. This type of mapping rule needs the mapping scheme of the secondary layer to be dependent on that of the basic layer (e.g., if two independently Gray mapped QPSK signals are added together, the superposed 16QAM is no longer entirely Gray mapped). However in the HM-based SFN, the constellation of the received signals can hardly be entirely Gray mapped. Fortunately, the constellation mapping rule for each transmitter in the SFN is very simple when adopting the structured SIC approach; it only requires the basic layer and secondary layer are independently Gray mapped. Refer back to the Equation (4.5), where the basic layer LLR calculation is only related to: (1) basic layer mapping itself; (2) the values of all possible secondary layer symbols (here we assume perfect knowledge of the instantaneous channel state information). Therefore the basic layer Gray mapping is enough to minimize the BER for the global data, and the same rule is also applied to the secondary layer decoding. This advantage reduces the mapping complexity in the implementation.

- Easy extension to the multi-carrier systems: The structured SIC approach described above is well suited to the multi-carrier systems (e.g., OFDM). In Section 4.5, the proposed structured SIC algorithm is evaluated in a real-world OFDM-based broadband digital radio (BRD) system.

4.4 Decoding Complexity Analysis and Comparisons

In this section, we analyze the computational complexity of the structured SIC approach, and compare it with that of the multi-layer iterative decoding approach.

The computation of the structured SIC approach mainly involves two parts:

- The LLR computation for the detectable signals in the SFN, which depends on the signal strengths and receiver sensitivity. The LLR for the basic layer coded bits calculated in the structure-based detector, which is illustrated in Fig. 4.3 and based

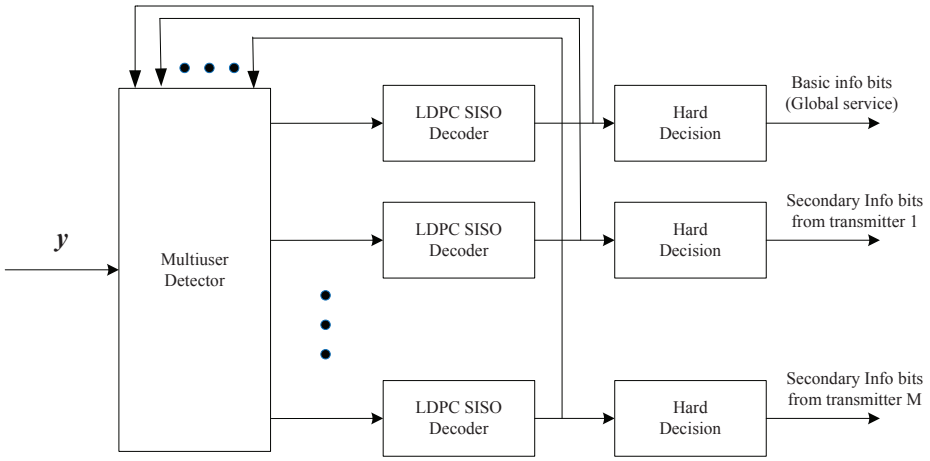

Figure 4.4: Block diagram of the LDPC multi-layer iterative receiver.

on Equation (4.5). The similar LLR calculation approach is applied to the secondary layer, when the mobile user is within the local service coverage.

- The iterations in the LDPC decoding.

The block diagram of the LDPC multi-layer iterative decoding is shown in Fig. 4.4 (the details of multi-layer iterative decoding can refer to [30][31]). The multiuser detector (MUD) outputs are connected to the soft inputs of $M+1$ parallel LDPC decoders (one decoder for global service data and M decoders for all the local service data), which produce the extrinsic soft outputs (the extrinsic information calculations are not shown in Fig. 4.4). Then the soft outputs of these decoders are fed back into the MUD, which can then improve its outputs along the iterations (the soft outputs of the decoders are used to aid each other). After enough iterations, the outputs are forwarded to the hard decision block to generate the final information bits for all layers (the global service data and M local service data). Due to the large signal power difference between the detectable signals and the other weak local signals, most of the weak local signals are not reliable, and we only focus on the reception of the detectable signals. The total computational complexity of the multi-layer iterative decoding approach is equal to the computational complexity of one iteration multiplying the number of iterations. For each iteration, the computational complexity mainly contains

two parts as shown in Fig. 4.4:

- The LLR of the MUD, which delivers the *a posteriori* LLR of a transmitted "1" and a transmitted "0" for every code bit of every layer (Equation (4) in [31]).

- The iterations in the LDPC decoding, which are the same as those of structured SIC.

Before we compare the computational complexity of the structured SIC approach with that of the multi-layer iterative decoding approach, some comparative prerequisites should be stated: the decoding complexity of the detectable signals for both approaches is compared in terms of: (1) the total number of operations on LLR computation; (2) the number of LDPC inner iterations for one LDPC block length. Keep in mind that the contribution for the number of operations on LLR computation is independent of its type, e.g., subtraction, multiplication, division, exponentiation and logarithm. In the case of complex operations, a complex multiplication is equivalent to four real multiplications plus two real additions, and each complex addition is equivalent to two real additions.

Table 4.1: Decoding complexity comparison; two transmitters broadcasts their own QPSK+QPSK HM signals over the SFN; the number of outside iterations for the multi-layer iterative decoding $N_{out} = 6$; the number of inner iterations in the LDPC decoder $N_{in} = 40$; L denotes one LDPC block length.

	number of operations on LLR computation	number of LDPC inner iterations
Multi-layer iterative decoding	$13896L$	720
Structured SIC (within local coverage)	$744L$ (reduction 94.6%)	80 (reduction 88.9%)
Structured SIC (out of local coverage)	$644L$ (reduction 95.3%)	40 (reduction 94.4%)

Let us take the decoding complexity of the detectable signals in Fig. 4.1 for example, where two transmitters are broadcasting their own QPSK+QPSK HM signals over the SFN.

The decoding complexity comparison results are summarized in Table 4.1. In this table, the number of LDPC decoder inner iterations N_{in} is set to be 40 for both approaches; the number of outside iterations N_{out} (between the LDPC decoder and MUD) is set to be 6 for the multi-layer iterative decoding approach; L denotes one LDPC block length; the basic layer and secondary layer of each transmitter are independently Gray mapped. As can be observed from Table 4.1, compared with the multi-layer iterative decoding approach, the structured SIC offers 94.6% computational saving on the LLR computation, and 88.9% saving on the number of iterations in the LDPC decoding when the mobile user is within the local service coverage (e.g., User2 in Fig. 4.1); the savings increase to 95.3% on the LLR computation, and 94.4% savings on the number of iterations in the LDPC decoding when the mobile user is out of the local service coverage (e.g., User1 in Fig. 4.1). In section 4.5 we will show that, with the much lower decoding complexity, the structured SIC approach still offers comparable BER performance of the detectable signals with that of multi-layer iterative decoding approaches in the HM-based SFN scenario.

4.5 Algorithm Implementation and Numerical Results

In this section, the algorithm implementation platform and settings are first introduced. And then we will compare the performance of the structured SIC approach with that of the multi-layer iterative decoding approach. The performance of the traditional SIC method (e.g., without taking account of the secondary layer structure information) is also provided as a reference.

4.5.1 Algorithm implementation and Settings

The structured SIC algorithm is applied to the BDR networks. The block diagram of the BDR transmitter (all the transmitters have the same structure in the SFN) and receiver are shown in the Fig. 4.5. The feature blocks of one BDR transmitter in the SFN include an LDPC encoder, a HM mapper and an OFDM modulator. For performance evaluation, we use a practical case, where two BDR stations (station1 and station2) are broadcasting QPSK+QPSK HM signals over the SFN (e.g., Fig. 4.1). In this two-transmitter HM based

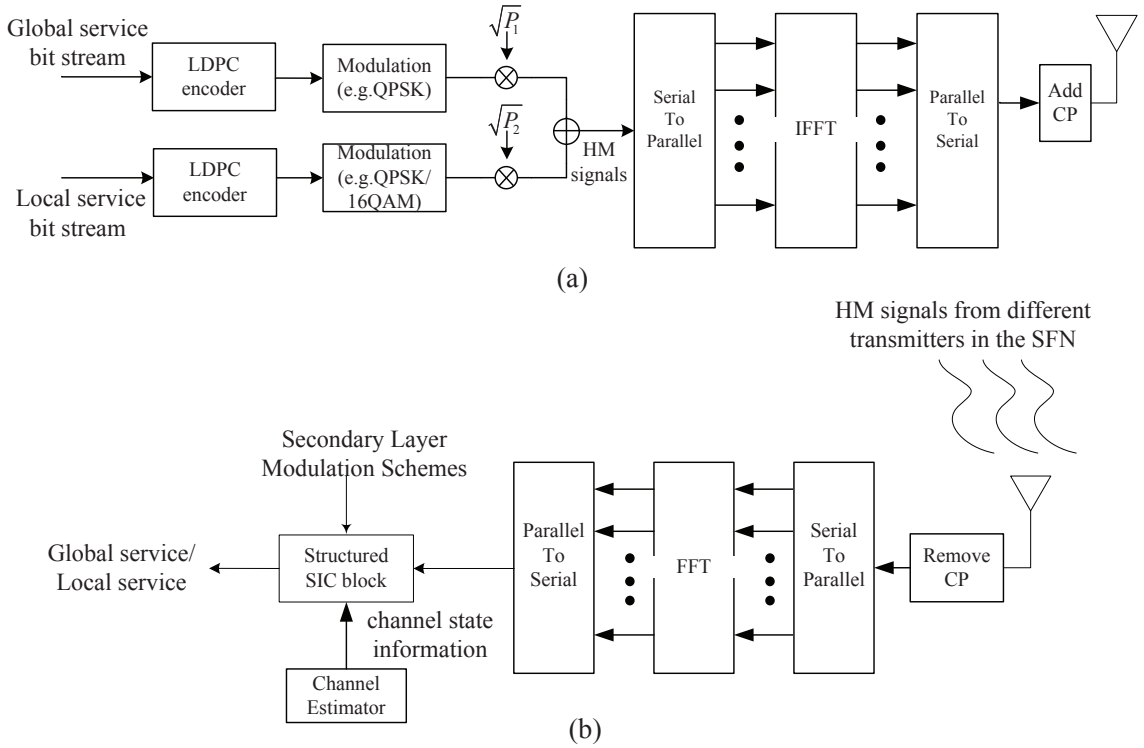

Figure 4.5: (a) A BDR transmitter block diagram; (b) The BDR receiver block diagram, the receiver decodes the global and local service data based on the HM signals from different BDR transmitters in the SFN.

SFN, the received signal can be written as

$$\begin{aligned} y &= h_1 s_1 + h_2 s_2 + n \\ &= h_1(\sqrt{P_{1,1}}x_1 + \sqrt{P_{1,2}}x_{1,2}) + h_2(\sqrt{P_{2,1}}x_1 + \sqrt{P_{2,2}}x_{2,2}) + n \\ &= (h_1\sqrt{P_{1,1}} + h_2\sqrt{P_{2,1}})x_1 + h_1\sqrt{P_{1,2}}x_{1,2} + h_2\sqrt{P_{2,2}}x_{2,2} + n \end{aligned} \tag{4.8}$$

with $\sqrt{P_{1,1}} + \sqrt{P_{1,2}} = P_1$ and $\sqrt{P_{2,1}} + \sqrt{P_{2,2}} = P_2$, where P_1 and P_2 are the received signal power from BS1 and BS2, respectively.

The received signal contains three different components: the same basic layer signals x_1 and two secondary layer signals $x_{1,2}$ and $x_{2,2}$. We defined the carrier to noise ratio as

$$\mathbf{C/N} = \frac{\left\|h_1\sqrt{P_{1,1}} + h_2\sqrt{P_{2,1}}\right\|^2 + \left\|h_1\sqrt{P_{1,2}}\right\|^2 + \left\|h_2\sqrt{P_{2,2}}\right\|^2}{\sigma^2}, \tag{4.9}$$

where σ^2 is the variance of additive white Gaussian noise.

Let λ_1 and λ_2 be the power ratio between the basic layer signal and the secondary layer for the two BDR stations, respectively.

$$\lambda_1 = \frac{P_{1,1}}{P_{1,2}} \text{ and } \lambda_2 = \frac{P_{2,1}}{P_{2,2}}. \tag{4.10}$$

The received signal power ratio between the station1 and the station2 is defined as

$$\lambda = \frac{\|h_1\|^2 P_1}{\|h_2\|^2 P_2}. \tag{4.11}$$

In the BDR networks, we do not differentiate the power ratios of two BDR stations, thus in the following performance evaluation we set $\lambda_1 = \lambda_2 = \lambda_{1,2}$. Other simulation related parameters are: the LDPC code length is 9216 - details of the LDPC codes are defined in CMMB specifications [33]; the code rate is 3/4; the number of OFDM subcarriers is 2048; the QPSK signal of the basic layer and secondary layer are independently Gray mapped; we assume perfect knowledge of the instantaneous channel state information in the simulations.

4.5.2 BER Performance Comparisons

We classify the signal receptions into two cases in terms of the mobile user's location: (1) out of the the local service coverage (e.g., User1 in Fig. 4.1); (2) within the local service coverage (e.g., User2 in Fig. 4.1). In the corresponding two tables, we compare the required minimum $\mathbf{C/N}$ (BER less than 10^{-4}) for the detectable signals transmission when using different decoding approaches.

Case 1 *Mobile user is out of the local service coverage*

In this case, the global service data is the detectable signal. λ is set to be 0 dB in the simulation, which indicates the mobile user is in the middle of the two stations and receives the same signal strength from two stations. We evaluate the performance of different decoding approaches under different $\lambda_{1,2}$. The minimum required $\mathbf{C/N}$ values for the global service transmission are listed in Table 4.2. When $\lambda_{1,2}$ is 3 dB, our proposed structured SIC approach can provide 0.2 dB gain compared to the traditional SIC approach under AWGN channel; while the gain increases to 0.6 dB under Rayleigh fading channel. Compared with

Table 4.2: Required minimum C/N for the global service transmission to achieve a BER = 1×10^{-4} when the mobile user is out of local service coverage.

	Channel model	C/N for global service (dB)	
		$\lambda_{1,2} = 3\,dB$	$\lambda_{1,2} = 6\,dB$
Traditional SIC	AWGN	9.7	6.9
Multi-layer Iterative decoding		9.5	6.9
Structured SIC		9.5	6.9
Traditional SIC	Rayleigh	12.2	8.6
Multi-layer Iterative decoding		11.6	8.5
Structured SIC		11.6	8.5

the multi-layer iterative decoding approach, the structured SIC approach achieves the same **C/N** values for the global service transmission under both channel models. However the multi-layer iterative decoding approach needs a large number of iterations, which cost high decoding complexity and long delay. When $\lambda_{1,2}$ increases to 6 dB, all decoding approaches have the same detection threshold for the global service transmission under AWGN channel, and only 0.1 dB difference under Rayleigh fading channel. This is not surprising since the local service signals become weaker as $\lambda_{1,2}$ becomes larger, thus the weak local service signal result in less interference when decoding the global service data.

Case 2 *Mobile user is within the local service coverage of the neighboring station*

In this case, the detectable signals are the global service data and one local service data from the neighboring station. λ is set to be 6 dB in the simulation, indicating the received signal strength from station1 is 6 dB stronger than that from station2. The minimum required **C/N** values for both the global service and local service transmissions are listed in Table 4.3.

For the global service transmission, when $\lambda_{1,2}$ is 3 dB, the structured SIC approach can provide 0.2 dB gain under AWGN channel compared with the traditional SIC approach; while the gain increases to 0.7 dB under Rayleigh fading channel. Compared with the multi-layer iterative decoding approach, the structured SIC approach provides the same

Table 4.3: Required minimum C/N for both the global service and local service transmissions to achieve a BER $= 1 \times 10^{-4}$ when the mobile user is within the local service coverage of the the neighboring station.

	Channel model	C/N for global service (dB)		C/N for local service (dB)	
		$\lambda_{1,2} = 3\,dB$	$\lambda_{1,2} = 6$	$\lambda_{1,2} = 3\,dB$	$\lambda_{1,2} = 6\,dB$
Traditional SIC	AWGN	10.3	7.1	16.0	18.5
Multi-layer Iterative decoding		10.1	7.1	15.8	18.3
Structured SIC		10.1	7.1	15.8	18.3
Traditional SIC	Rayleigh	12.7	8.9	N/A	N/A
Multi-layer Iterative decoding		11.9	8.8	20.0	22.6
Structured SIC		12.0	8.8	20.1	22.7

performance under AWGN channel, and 0.1 dB less gain under Rayleigh fading channel; When $\lambda_{1,2}$ increases to 6 dB, the minimum required $\mathbf{C/N}$ values for the global service transmission decrease for all the decoding approaches (the weaker local service signals results less interference). The structured SIC approach provides the same performance as the multi-layer iterative decoding under both channel models; and meanwhile offers 0.1 dB gain compared with the traditional SIC approach under Rayleigh fading channel.

For the local service transmission, when $\lambda_{1,2}$ is 3 dB, the detection threshold of the structured SIC approach is 0.2 dB better than that of the traditional SIC approach under AWGN channel. Note that, the traditional SIC fails in the local service detection under Rayleigh fading channel (the local service signal from the other station results in the ICI), while the structured SIC approach still successfully detects the local service signal in this case. Compared with the multi-layer iterative decoding approach, the structured SIC provides the same performance under AWGN channel, and 0.1 dB less gain under Rayleigh fading channel; When $\lambda_{1,2}$ increases to 6 dB, the minimum required $\mathbf{C/N}$ values for the local service transmission increase for all decoding approaches (the ICI from the other station becomes weaker), but the benefits offered by the structured SIC approach still exist.

To summarize, compared with the traditional SIC approach, the structured SIC approach can offer 0-0.7 dB $\mathbf{C/N}$ gain for the global service transmission; and it can even detect the local service signal when the traditional SIC approach fails. Also it provides the comparable performance with the multi-layer iterative decoding (only 0.1 dB less gain for certain cases). Together with the decoding complexity comparisons, it reveals that the structured SIC approach achieves an excellent performance-complexity trade-off, especially for the HM-based SFN scenario.

4.6 Conclusions

A low-complexity decoding algorithm for the HM-based SFN is proposed in this chapter. By exploiting the mapping information of the secondary layers, the proposed structured SIC approach effectively mitigates the ILI and ICI in the SFN. Numerical results and decoding complexity analysis are provided to illustrate the efficacy of the proposed technique, which can be implemented in the HM-based SFN scenario with promising performance and low complexity.

Chapter 5

SYSTEM PROTOTYPE AND PERFORMANCE ANALYSIS

In this chapter, A BDR prototype has been built on the software defined radio (SDR) platform. Both the numerical simulations and preliminary lab results demonstrate significant performance advantage of the BDR.

5.1 Performance Analysis

Performance of the BDR system is evaluated under various multipath fading channels. The channel models used are the multipath propagation profiles for the VHF band, which are defined in DRM specifications [3]. The BER performance of the BDR system in AWGN, the Urban channel at 2 km/h (UB2) and 60 km/h (UB60), and the Rural channel at 150 km/h (Rr150), are plotted in Fig. 5.1 and Fig. 5.2. In addition, the BDR performance with and without frequency hopping are both simulated and compared. From Fig. 5.1 and Fig. 5.2, it is clear that frequency hopping significantly improves the system performance, especially in low mobility channels. For example in Urban channel at 2 km/h pedestrian speed, the C/N gain introduced by frequency hopping is 11.5 dB for QPSK with 1/3 code rate and 8.4 dB for 16-QAM with 1/2 code rate (for BER at 10^{-4} and lower).

Performance comparison between the BDR and the DRM systems is listed in Table 5.1 and Table 5.2. As observed, the detection threshold of BDR signals is 0.1-3.1 dB better than that of DRM in medium and high mobility channels. The performance of DRM in low mobility channels is not published. It is reasonable to believe that the BDR has even greater advantage over DRM in low mobility channels due to the incorporation of frequency hopping. Table 5.3 summarizes the data rates of BDR, DRM and HD Radio systems. By aggregating multiple bands into a wider band, the maximum data rate supported by BDR is more than 8 times higher than those of DRM and HD Radio.

The required minimum C/N (BER less than 10^{-4}) values for hierarchical modulated

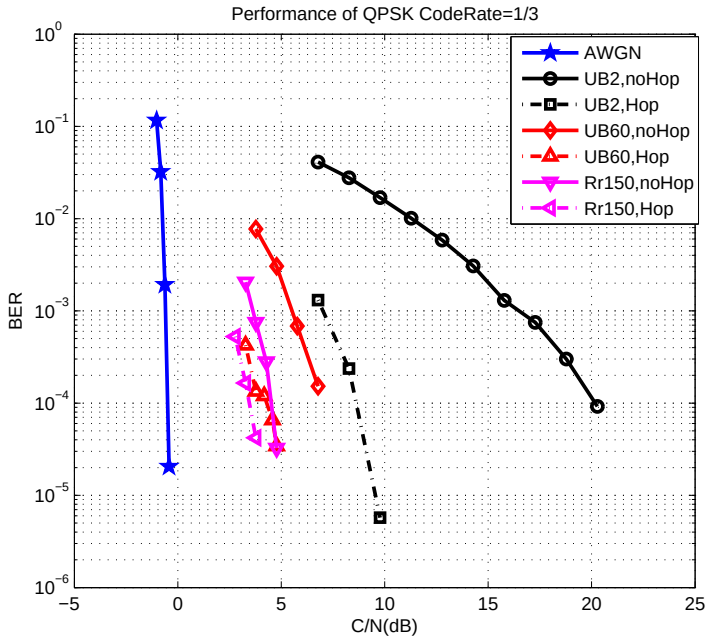

Figure 5.1: Performance of BDR in various multipath channels with and without frequency hopping (QPSK with rate 1/3 code).

Table 5.1: Required C/N for a transmission to achieve a BER $= 1 \times 10^{-4}$, QPSK with 1/3 code rate

Channel model	DRM	BDR(no hop)	BDR(hop)
AWGN	1.3 dB	-0.5 dB	-0.5 dB
Urban at 2km/h	N/A	20.1 dB	8.6 dB
Urban at 60km/h	7.3 dB	6.9 dB	4.3 dB
Rural at 150km/h	5.6 dB	4.5 dB	3.4 dB

BDR signals are provided in Table 5.4 and Table 5.5 under different power ratio λ (between the basic and the secondary layers). In both the QPSK+QPSK case and the QPSK+16QAM case, the signals are protected with LDPC of 1/2 code rate - details of the LDPC codes are defined in CMMB specifications [33].

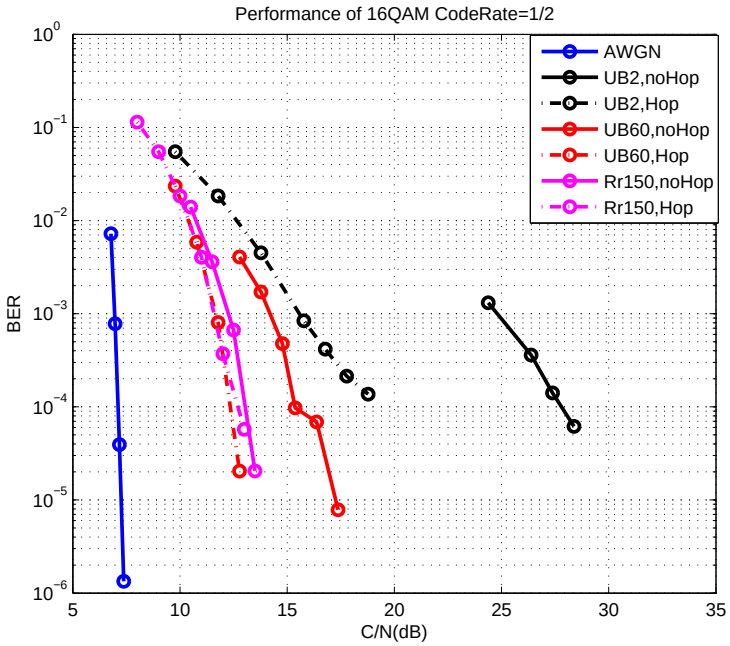

Figure 5.2: Performance of BDR in various multipath channels with and without frequency hopping (16-QAM with rate 1/2 code).

Table 5.2: Required C/N for a transmission to achieve a BER $= 1 \times 10^{-4}$, 16-QAM with 1/2 code rate

Channel model	DRM	BDR(no hop)	BDR(hop)
AWGN	7.9 dB	7.2 dB	7.2 dB
Urban at 2km/h	N/A	27.7 dB	19.3 dB
Urban at 60km/h	15.4 dB	15.3 dB	12.3 dB
Rural at 150km/h	13.1 dB	12.9 dB	12.7 dB

Since the performance of DRM in hierarchical modulation is not published, performance comparison between the BDR and the DVB-T systems is listed in Table 5.6. In [15], the constellation of hierarchical modulation is specified by the parameter α, which represents the ratio between the spacing of two adjacent constellation points of two neighboring quadrants

Table 5.3: Data rate comparison

Modulation	Code rate	DRM(kbps)	BDR without aggregation(kbps)	BDR with aggregation(kbps)
QPSK	1/4	37.3	35.1	280.8
QPSK	1/3	49.7	46.8	374.4
QPSK	1/2	74.5	70.3	562.4
QPSK	3/4	N/A	105.4	843.2
16QAM	1/4	N/A	70.3	562.4
16QAM	1/3	99.4	93.7	749.6
16QAM	1/2	149.1	140.6	1124.8
16QAM	3/4	N/A	210.8	1686.4
64QAM	1/4	N/A	79.1	632.8
64QAM	1/3	N/A	105.5	844.0
64QAM	1/2	N/A	158.2	1265.6
64QAM	3/4	N/A	316.3	2530.4

Table 5.4: Required C/N for the basic layer and secondary layer transmission to achieve a BER $= 1 \times 10^{-4}$, QPSK+QPSK with 1/2 code rate

$\lambda(dB)$	Basic layer (dB)	Secondary layer (dB)
3	7.7	7.7
6	4.0	8.9
9	2.5	11.5
12	1.9	14.2
15	1.5	17.1
∞	1.2	N/A

Table 5.5: Required C/N for the basic layer and secondary layer transmission to achieve a BER $= 1 \times 10^{-4}$, QPSK+16QAM with 1/2 code rate

$\lambda(dB)$	Basic layer (dB)	Secondary layer (dB)
3	8.0	11.1
6	4.5	13.3
9	3.1	15.7
12	2.6	18.5
15	2.3	21.6
∞	1.2	N/A

and the spacing of two adjacent constellation points within quadrant. Essentially, α and the power ratio λ used in this proposal measure the same relation - both representing the power allocation ratio in the hierarchical modulation. In Table 5.6, we compare the required minimum C/N for the basic layer in hierarchical modulation between the BDR and the DVB-T systems.

As it can be observed in Table 5.6, for the QPSK+QPSK transmission scheme the detection threshold of basic layer BDR is 2.2-2.7 dB better than that of DVB-T system under AWGN channel, and 2.9-4.2 dB better under Rayleigh fading channel. For the QPSK+16QAM transmission scheme, the detection threshold of basic layer BDR is 2.6-2.9 dB and 3.1-4.5 dB better than that of DVB-T system under the AWGN and Rayleigh fading channel, respectively. This is quite significant in light of the fact that the hierarchical modulation schemes used in the two systems are virtually identical.

5.2 Laboratory Tests

In addition to numerical evaluations, a BDR prototype has been built on the Microsoft Research Software Radio (Sora) [5] , which is a powerful software radio with full programmability on commodity PC platforms. A picture of the Sora testbed is shown in Fig. 5.3. As typically seen in software defined radio, a common high performance RF front-end

Table 5.6: Comparison of the required minimum C/N in the basic layer transmission for hierarchical modulation between BDR and DVB-T

Modulation Scheme	$\lambda(dB)$	Code rate	AWGN channel (dB)		Rayleigh Channel (dB)	
			BDR	DVB-T	BDR	DVB-T
QPSK+QPSK	9.54	1/2	2.4	5.1	4.6	7.7
	($\alpha = 2$)	3/4	6.1	8.6	10.0	14.2
QPSK+QPSK	13.97	1/2	1.7	4.1	3.7	6.6
	($\alpha = 4$)	3/4	4.9	7.1	9.0	13.1
QPSK+16QAM	5.05	1/2	5.1	8.5	7.7	11.8
	($\alpha = 1$)	3/4	11.1	15.0	14.8	19.3
QPSK+16QAM	6.99	1/2	3.9	6.5	6.3	9.4
	($\alpha = 2$)	3/4	8.2	11.1	12.1	16.3

(VHF in our case) is used to convert the RF signal to digital baseband. Peculiar in Sora is the fact that the sampled signals are directly connected to the PC through a radio control board (RCB). The interface between RCB and PC is PCIe, which supports a throughput up to 12.8 Gbps (PCIe x8). The digital samples are processed on general purpose multi-core processors, which are both powerful and scalable. To meet the requirement of real-time processing, the DSP tasks are partitioned and streamlined on multiple CPU cores. Several processing tasks with intensive computation complexity, such as the up and down sampling, Fast Fourier Transform (FFT) and LDPC decoding, are optimized by taking advantage of the data-parallelism with the Single Instruction Multiple Data (SIMD) instruction sets of the CPU.

In the lab testing environment, the BDR transmitter and receiver implemented on two PCs are connected through a channel fading simulator. By adjusting the additive noise power, the bit error rate (BER) of the demodulated signal is measured and the carrier to noise ratio (C/N) is recorded when BER exceeds 10^{-4}. The constellations (after equalizer) of 16-QAM and QPSK+QPSK hierarchical modulation under AWGN channel are shown

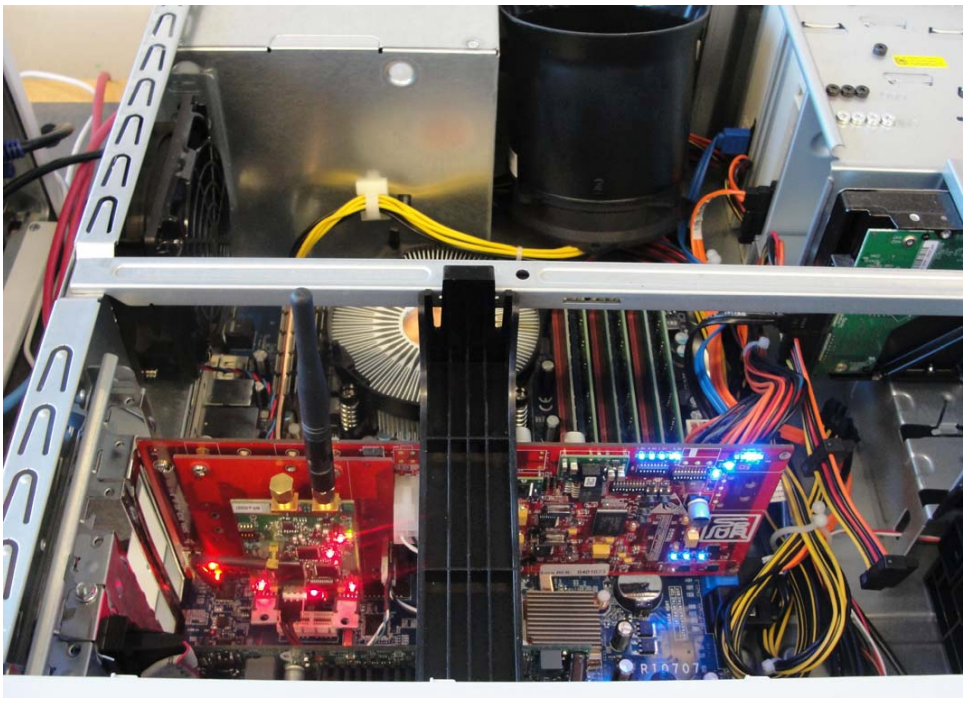

Figure 5.3: A picture of the SORA platform

in Fig. 5.4 and Fig. 5.5, respectively. To achieve a BER of 10^{-4} in AWGN channel, the required C/N for QPSK with 1/3 code rate and 16-QAM with 1/2 code rate are 0 dB and 7.9 dB, respectively. These numbers correspond to implementation losses of only 0.5 dB and 0.7 dB, respectively (relative to the simulation results in Table 5.1 and Table 5.2).

After the functional verification on the SDR, a BDR prototype on the field programmable gate array (FPGA) platform has been completed recently. The lab tests (shown in Fig. 5.6) and field trials are being conducted in Shanghai currently. The digital audio commercial networks, which involve digital conversion of nineteen analog radio stations, will be launched in Guangdong province in early 2013.

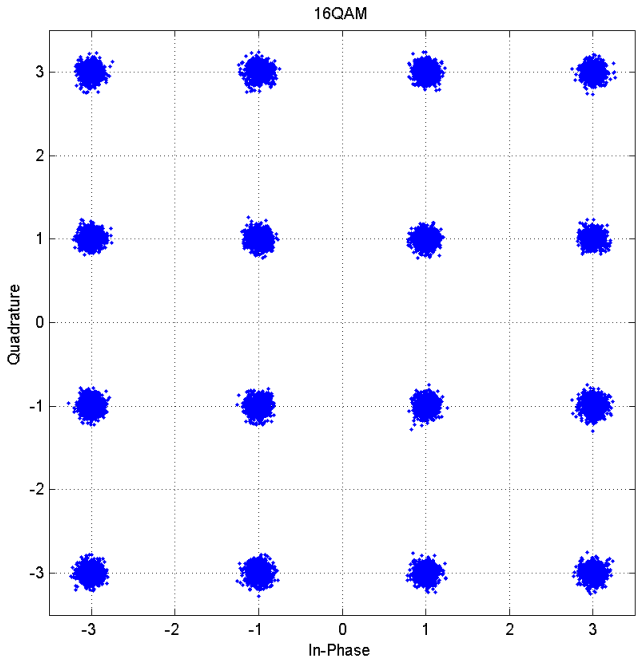

Figure 5.4: 16-QAM under AWGN channel simulator

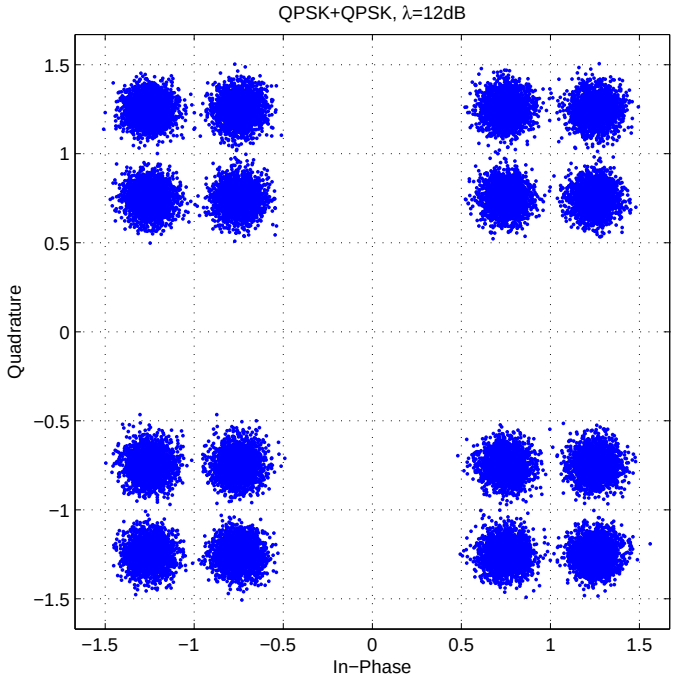

Figure 5.5: QPSK+QPSK hierarchical modulation under AWGN channel simulator

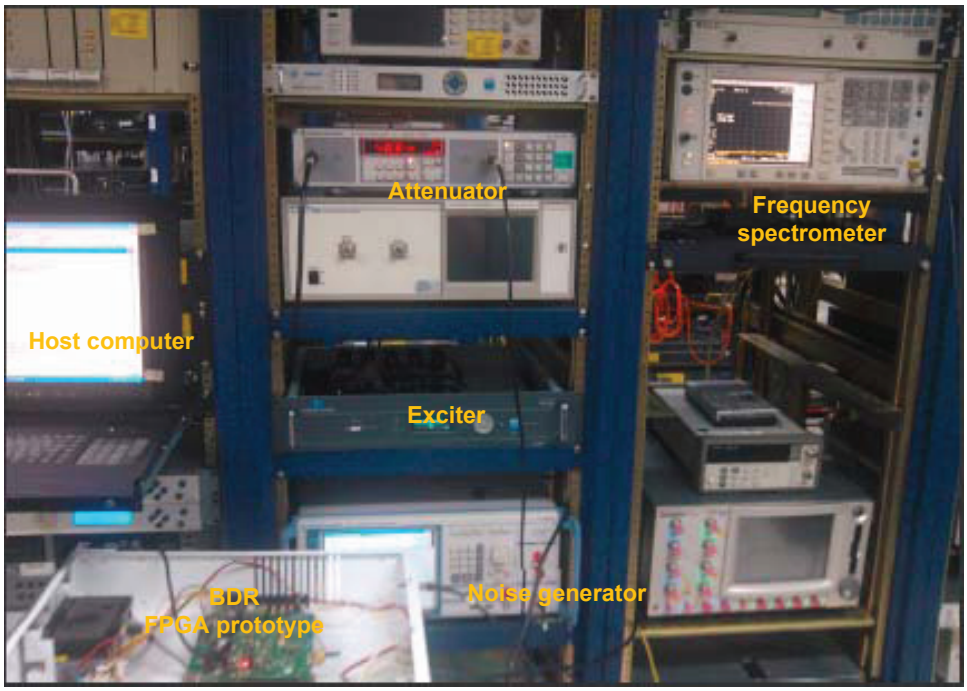

Figure 5.6: The BDR FPGA prototype

Chapter 6

CONCLUSION AND FUTURE WORK

6.1 Conclusion

This dissertation focuses on the enabling technologies for broadband in-band on-channel (IBOC) digital radio. We have developed a broadband digital radio (BDR) specification that meets and exceeds the specific set of requirements in IBOC broadcasting. The new digital broadcasting system offers: (a) better and richer user experiences than the traditional analog broadcasting with smaller bandwidth; (b) compatibility/coexistence with existing analog radio stations; (c) more multimedia features specifically for the Chinese market (e.g., audio/video reception in the high-speed vehicle, audio sideshows with image and animation); (d) bandwidth flexibility from 100 KHz up to 800 KHz. Our contributions are summarized below.

1. The entire system architecture design. By synergistically combining the LDPC codes, the band aggregation and the frequency hopping techniques, as well as an efficient hierarchical modulation scheme, BDR offers both performance and services advantages in various application scenarios. On the service side, the BDR supports a wider range of data rate (up to 2.53 Mbps) and is capable of delivering high quality radio and rich multi-media services such as data, image and video.

2. A Novel LDPC Decoding Algorithm for Hierarchical Modulation. We have developed a novel LDPC decoding algorithm for the coded hierarchical demodulation signals, in which the LDPC decoder is refined to account for the non-Gaussian interference from the second layer. The method greatly enhances the BDR performance of hierarchical modulation in both AWGN and fading channels over DVB-T system.

3. A BDR prototype on the powerful software radio platform. The initial laboratory

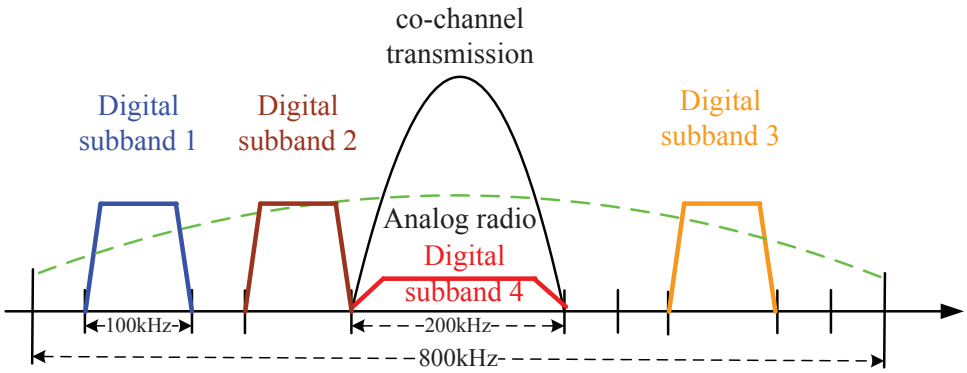

Figure 6.1: Digital band 4 shares the same channel with the analog station.

tests demonstrate significant performance advantages of the new design over existing systems such as the Digital Radio Mondiale (DRM) and Hybrid Digital (HD) radio.

6.2 Future Work

6.2.1 Dirty paper coding technique for co-channel transmission

In order to further increase the data rate and utilize the analog radio spectrum more efficiently, we will consider the scenario where the digital and analog signal can be transmitted using the same channel. For example, in Fig. 6.1 the digital band 4 shares the same channel with the analog station. In the co-channel case, the dirty-paper coding (DPC) is needed to enable the analog-interference-free reception of the digital signal.

Dirty paper coding was introduced by M. Costa in 1983. A well-known practical DPC implementation approach is the Tomlinson-Harashima precoding originally developed for the intersymbol interference (ISI) channels. Its simple structure makes THP a very attractive solution for DPC implementation. However it is shown that the THP suffers from the shaping loss, a modulo loss and a power loss (e.g., in high SNR region, THP suffers a 1.53dB capacity loss due to shaping). For the future work, we plan to adopt the lattice precoding to compensate the performance loss, the block diagram of the DPC procoder are shown in Fig. 6.2. The challenging point is that, the modulo loss is difficult to compensate in low SNR region (SNR$\leq$5 dB).

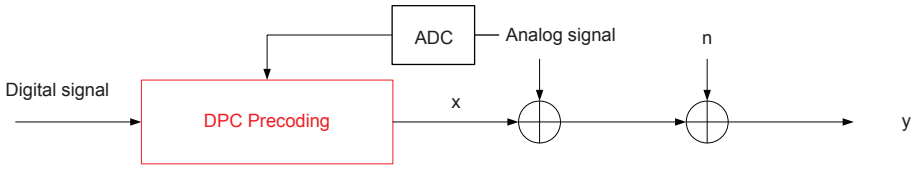

Figure 6.2: The block diagram of the DPC procoder.

6.2.2 Fountain code decoding

For one-to-one communication, ARQ was introduced as an effective and reliable error control mechanism which utilizes acknowledgments and timeouts to recover from packet losses. It achieves high throughput, low delay and in-order delivery in one-to-one communication. However its application is limited to unicast communication or broadcasting with small number of end users. It does not scale well due to so-called feedback implosion problem. Hence for broadcast communication, especially with large number of users, other solutions has been proposed in the literature. One of the most effective ways is to use the concept of erasure coding in which a source file of N packet is encoded into Z packets (Z can be infinity) and transmitted without any feedback from the receivers. As long as the receiver obtains N correct packets, it is able to decode the N source packets to recover the information packets.

In practice, however, there is usually limitation on number of packets the base stations (BTS) would transmit. Clearly, for a set of information packets, a BTS will not transmit infinite number of coded packets. Suppose a BTS finally receives N-1 correct packets and M wrong packets (in this case $Z = N + M - 1$), we plan to extract the extra correct packet from the M wrong packets to complete the decoding process.

BIBLIOGRAPHY

[1] Wolfgang Hoeg and Thomas Lauterbach, "Digital Audio Broadcasting: Principles and Applications of DAB, DAB + and DMB," Wiley Press, June 2009.

[2] D. Bodson, "Digital Audio Around the World," *IEEE Vehicular Technology Magazine*, Vol. 5, pp. 24-30, Dec. 2010.

[3] ETSI ES 201 980 v3.1.1 (2009-8), Digital Radio Mondiale (DRM); System Specification.

[4] D. P. Maxson, "The IBOC Handbook: Understanding HD Radio (TM) Technology," Focal Press, August 2012.

[5] K. Tan *et al*, "Sora: High Performance Software Radio using General Purpose Multi-core Processors," USENIX NSDI 2009, Apr 2009, Boston, MA.

[6] J. Ramos, M. Zoltowski, H. Liu, "Low-complexity space-time processor for DS-CDMA communications," *IEEE Transactions on Signal Processing*, Volume48, Issue 1, pp. 39-52, January, 2001.

[7] K. Li, H. Liu, "Joint channel and carrier offset estimation in CDMA communications," *IEEE Transactions on Signal Processing*, vol. 47, issue 7, pp 1811-1822, July, 1999.

[8] Z. Kostic, I. Maric, and X. Wang, "Fundamentals of dynamic frequency hopping in cellular systems," *IEEE Journal on Selected Areas in Communications*, Vol 19, issue 11, pp. 2254-2266, 2001.

[9] D. J. C. MacKay, "Good error-correcting codes based on very sparse matrices," *IEEE Transactions on Information Theory*, vol.45, pp. 399-431, Mar. 1999.

[10] Mobile Multimedia Broadcasting (P. R. China) Part 1: Framing Structure, Channel Coding and Modulation for Broadcasting Channel.

[11] H. Jiang and P. Wilford, "A hierarchical modulation for upgrading digital broadcast systems," *IEEE Transactions on Broadcasting*, Vol. 51, No. 2 (2005), pp. 223-229.

[12] H. Schwarz, D. Marpe and T. Wiegand, "Overview of the scalable video coding extension of the H.264/AVC standard," *IEEE Transactions on Circuits and System.* Video. Technol., vol. 17, no. 9, pp. 1103–1120, Sept. 2007.

[13] Z. Hu and H. Liu, "Structure-based Decoding for Hierarchically Modulated, LDPC coded Signals," *IEEE GLOBECOM'12, California*, USA, 3-7 Dec. 2012.

[14] Digital Video Broadcasting (DVB): *Frame Structure, Channel Coding and Modulation for a Second Generation Digital Terrestrial Television Broadcasting System* (DVB-T2), EN 302 755 V.1.1.1., European Telecommunications Standard Institute ETSI, Sep. 2009.

[15] ETSI, EN 3000 744, V1.5.1, Digital Video Broadcasting (DVB): *framing structure, channel coding and modulation for digital terrestrial television*, November 2004.

[16] K. Ramchandran, A. Ortega, K. M. Uz and M. Vetterli, "Multiresolution broadcast for digital HDTV using joint source/channel coding," *IEEE J.Sel. Areas Commun.*, vol. 11, no. 1, pp. 6–23, Jan. 1993.

[17] M. J. Hossain, P. K. Vitthaladevuni, M.S. Alouini, and V. K. Bhargava, "Hierarchical modulations for multimedia and multicast transmission over fading channels," *IEEE Trans. Inf. Theory*, vol. 51, no. 1, pp. 154–172, Jan. 2005.

[18] A. Schertz and C. Weck, "Hierarchical modulation—The transmission of two independent DVB-T multiplexes on a single frequency," EBU Tech. Rev., pp. 1–13, Apr. 2003.

[19] H. Schwarz, D. Marpe and T. Wiegand, "Overview of the scalable video coding extension of the H.264/AVC standard," *IEEE Trans. Circuits.Syst.* Video. Technol., vol. 17, no. 9, pp. 1103–1120, Sept. 2007.

[20] D. Wu, Y. T. Hou and Y.Q. Zhang, "Scalable video coding andtransport over broadband wireless networks," *Proc.* IEEE, vol. 89, no. 1, pp. 6–20, Jan. 2001.

[21] S. Wang, S. Kwon and Yi, B.K., "On enhancing hierarchical modulation," *IEEE International Symposium on Broadband Multimedia Systems and Broadcasting*, March 31 2008-April 2 2008, Las Vegas, NV, (2008), pp. 1-6.

[22] J. Wu, "Non-uniform and large distance constellation design for hierarchical modulation," *2010 IEEE International Conference on Communications (ICC)*, May 23 2010, Cape Town, pp. 1-5.

[23] B. Liu, H. Li, H. Liu and S. Roy, "DPC-based hierarchical broadcasting: Design and implementation," *IEEE Trans. Veh. Tech.,* Nov. 2008, pp. 3895-3900.

[24] X. Zhe, W. YongSheng, F. Alberge and P. Duhamel, "A turbo Iteration Algorithm in 16QAM Hierarchical Modulation," *Proc. of IEEE Conf. on Wireless Communication Networking and Information Security*, 2010 June, pp. 9 – 12

[25] R. Dinis, J. C. Silva, N. Souto and P. Montezuma, "On the Design of Turbo Equalizers for SC-FDE Schemes with Different Error Protections," *2010 IEEE Vehicular Technology Conference Fall* (VTC 2010-Fall), 2010, pp. 1 – 5

[26] N. Souto, J. C. Silva, R. Dinis, F. Cercas, A. Correia, "An Iterative Receiver for WCDMA Systems with MIMO Transmissions and Hierarchical Constellations," 2006 IEEE Ninth International Symposium on Spread Spectrum Techniques and Applications, 2006, pp. 233 – 237

[27] N. Souto, F. Cercas, R. Dinis, J. C. Silva, A. Correia, "Transmitter/Receiver Method for Supporting Hierarchical Modulations in MBMS Transmissions," *Wireless Personal Communications Journal* (WIRE), Springer Press, Volume 45, No 1, April 2008.

[28] R. Juang, P. Ting, K. Lin, H. Lin and D. Lin, "Enhanced hierarchical modulation with interference cancellation for OFDM systems," International Symposium on Personal, Indoor and Mobile Radio Communications, pp. 217-220, 2009.

[29] D. Tse and P. Viswanath, Fundamentals of Wireless Communication. Cambridge University Press, May 2005.

[30] X. Wang and H.V. Poor, "Iterative (Turbo) Soft Interference Cancellation and Decoding for Coded CDMA," *IEEE Trans. on Comm.*, 46(7), pp.1046-1061, July 1999.

[31] A. Sanderovich, M. Peleg and S. Shamai, "LDPC coded MIMO multiple access with iterative joint decoding," *IEEE Trans. Info. Theory*, vol. 51, no. 4, Apr. 2005, pp. 1437–1450.

[32] H. Jiang and P. Wilford, A hierarchical modulation for upgrading digital broadcast systems, *IEEE Trans. on broadcasting*, Vol. 51, No. 2 (2005), pp. 223-229.

[33] Mobile Multimedia Broadcasting (P. R. China) Part 1: Framing Structure, Channel Coding and Modulation for Broadcasting Channel.

[34] Z. Hu, X. shao, Z. Chen, G. Xing and H. Liu, "System design and implementation of Broadband In-Band On-Channel Digital Radio," *2012 IEEE International Conference on Communications (ICC)*, Ottawa, Canada, June 10-15, 2012.

[35] E. R. William and S. Lin, *Channel codes classical and modern.* Cambridge University Press, 2009.

[36] V. Mignone, A. Morello and M. Visintin, "An Advanced Algorithm for Improving DVB-T Coverage in SFN", in *Proc. International Broadcasting Convention*, Sept. 1997, pp. 534-540.

[37] A. Mattsson, "Single frequency networks in DTV," *IEEE Trans. on broadcasting*, vol. 51, no. 4, pp. 413–422, Dec. 2005.

[38] R. Rebhan and J. Zander, "On the outage probability in single frequency networks for digital broadcasting," *IEEE Trans. on broadcasting*, vol. 39, no. 4, pp. 395–401, Dec. 1993.

[39] D. Plets *et al.*, " On the Methodology for Calculating SFN Gain in Digital Broadcast Systems," *IEEE Trans. on broadcasting*, vol. 56, no. 3, pp. 331 - 339, Sept. 2010.

[40] A. Ligeti and J. Zander, "Minimal cost coverage planning for single frequency networks," IEEE Trans. Broadcast., vol. 45, no. 1, pp. 78–87, Mar. 1999.

[41] G. May and P. Unger, "A New Approach for Transmitting Local Content Within Digital Single Frequency Broadcast Networks," *IEEE Transactions on Broadcasting*, vol. 4, no. 53, pp. 732–737, December 2007.

[42] Framing Structure, Channel Coding and Modulation for Satellite Services to Handheld Devices (SH) Below 3 GHz, ETSI EN 302 583 V1.1.1 (2008-03), Digital Video Broadcasting (DVB).

[43] H. Jiang, P. Wilford and S. Wilkus, Providing Local Content in a Hybrid Single Frequency Network Using Hierarchical Modulation, *IEEE Transactions on Broadcasting*, vol. 56, pp. 532 – 540, 2010

[44] J. Lopez-Sanchez, C.R. Ruescas, D. Gomez-Barquero and N. Cardona, "Provision of Local and Mobile Services in DVB-T Networks," *IEEE Latin-American Conference on Communications (LATINCOM)*, Sept. 2010, pp. 1-6.

[45] M. Feng, X. She and L. Chen, "A Novel Retransmission Scheme for Hierarchical Modulation Based MBMS," *IEEE Vehicular Technology Conference*, 2009, pp. 1-6.

[46] P. Unger and T. Kurner, "Spectrum optimization in DVB-H single frequency networks with local service areas ," *IEEE International Symposium on Broadband Multimedia Systems and Broadcasting*, pp. 1–6, 2008.

[47] J. Zoellner, J. Robert, S. Atungsiri and M. Taylor, "Local Service Insertion in Terrestrial Single Frequency Networks Based on Hierarchical Modulation," *IEEE International Conference on Consumer Electronics*, 2012, pp. 616-617.

[48] A. Goldsmith, Wireless Communications, Cambridge University Press, 2005.

[49] D. Bodson, "Digital Audio Around the World," *IEEE Vehicular Technology Magazine*, Vol. 5, pp. 24-30, Dec. 2010.

VITA

Zixia Hu received his B.S. in Information Engineering with Honors from Southeast University, Nanjing, China, in 2006, the M.S. degree in Electrical Engineering from Delft University of Technology, Delft, Netherlands in 2009 (Fudan-TU Delft International Cooperative Project, First Place), the M.S. degree in Microelectronics from Fudan University, Shanghai, China, in 2009. From April 2008 to March 2009, he worked as an research intern with ST-Ericsson Research Lab, Eindhoven, Netherlands, focusing on IEEE 802.15a UWB-OFDM system. Since fall of 2009, he started to work toward the Ph.D degree in the Electrical Engineering Department at University of Washington, Seattle, Washington, USA. During Ph.D study, he was a graduate research assistant in the Wireless Information Technology lab at University of Washington. In June of 2012, he also received a M.S. degree in Applied Mathematics at University of Washington. Now he is working in the DSP Group at Marvell semiconductor as a senior system engineer, focusing on IEEE 802.15 Smart Utility Networks (SUN) system design. His current research interests include the areas of communication theory and statistical signal processing, wireless system design and implementation.